DØ Note 5269, v2.10 (October 29, 2006)

Measurement of $p\bar{p} \to \mu^+\mu^-$ yield in the Z mass region for DØ Run 2A data

Angela Bellavance, Kristian Harder, Carsten Hensel, Gavin Hesketh, Norik Khalatyan, Alexandre Lobodenko, Dmitry Onoprienko, and Heidi Schellman

Abstract

A measurement of the Z vector boson yield in the muon channel at DØ is described.

1 Introduction

We describe an analysis of Z $\rightarrow \mu^+\mu^-$ in p$\bar{\text{p}}$ collisions at 1.96 TeV collected with the DØ detector over the entire period of run 2A. The analysis updates that described in DØ note 4573 and 4689[1], with differences in purpose, scope, and technique.

A basic goal of this work is to obtain values of $Y_Z\left(r,r'\right) \equiv \sigma_{Z/\gamma} B_{Z\rightarrow\mu\mu} \cdot \mathcal{L}\left(r,r'\right)$, where $Y_Z\left(r,r'\right)$, the yield, is the fully corrected number of $p\bar{p} \rightarrow \mu^+\mu^-$ events with dimuon invariant mass 60 GeV/c^2 $< M_{\mu\mu} <$ 130 GeV/c^2 produced between runs r and r', $\mathcal{L}\left(r,r'\right)$ is the integrated luminosity in the experiment between runs r and r', and $\sigma_{Z/\gamma} B_{Z\rightarrow\mu\mu}$ is the inclusive cross section for $p\bar{p} \rightarrow Z^0/\gamma^* \rightarrow \mu^+\mu^-$. Using the theoretical value $\sigma_{Z/\gamma} B_{Z\rightarrow\mu\mu}$ allows a $\sim 5\%$ determination of the luminosity that is largely independent of the DØ luminosity monitor.

Using $\mathcal{L}_{tot}$, the total integrated luminosity of Run 2A measured by the luminosity monitors, the analysis will also yield a precision measurement of $\sigma_{Z/\gamma} B_{\mu\mu}$ with a 1 fb^{-1} data set. Combining with a corresponding measurement in the W channel of $\sigma_W B_{W\rightarrow\mu\nu}$ will allow extraction of $R_{WZ} = \left[\sigma_W B_{W\rightarrow\mu\nu}\right] / \left[\sigma_Z B_{Z\rightarrow\mu\mu}\right]$, independent of luminosity to first order. This in turn can be used to infer the total width of the W, $\Gamma_{W,\text{tot}}$ by using the well-measured value of $B_{Z\rightarrow\mu\mu}$ from LEP and the theoretical values of W partial width to muons $\left[\Gamma_{W\rightarrow\mu\nu}\right]_{\text{theory}}$ and the cross section ratio $\left[\sigma_W/\sigma_Z\right]_{\text{theory}}$:

$$\Gamma_{W,\text{tot}} = \frac{\left[\sigma_W/\sigma_Z\right]_{\text{theory}} \left[\Gamma_{W\rightarrow\mu\nu}\right]_{\text{theory}}}{B_{Z\rightarrow\mu\mu}} \frac{1}{R_{WZ}}. \tag{1}$$

This analysis differs in many ways in its technical implementation from that in Ref. 1, which used the DØChunkAnalyze package on TMB data from the contemporary WZ group inclusive muon skim [7].

- The analysis is based on the `2MUhighpt` TMB skim created and maintained by the Common Samples Group.

- CAFe is used for event selection. The CAFtrees are created from the `2MUhighpt` TMB skim with p18.07.00 TMBAnalyze and bug fixes that allow checks for floating point exceptions (division by zero, square roots of negative numbers) during CAFtree production, which are commonplace in standard Common Samples Group CAFtrees. Data and Monte Carlo (MC) CAFtrees are produced with the same code. The number of events and thus the integrated luminosity of corresponding TMB and CAFtree samples are exactly identical. Efficiency measurements are still done with `Wzreco/muo_cert` on TMB because there is no adequate CAF-based replacement available yet.

- All MC events use the full GEANT simulation (no PMCS), versions p17.09.01 and p17.09.06. p17.09.01 MC is also used for simulation of $\gamma/Z \rightarrow \mu^+\mu^-$ and $\gamma/Z \rightarrow \tau^+\tau^-$ events in off-peak invariant mass ranges that contribute only weakly to the yield measurement ($15\,\text{GeV}/c^2 < M_{\mu\mu} < 60\,\text{GeV}/c^2$, $130\,\text{GeV}/c^2 < M_{\mu\mu} < 1000\,\text{GeV}/c^2$).

- Extensive use is made of re-weighting to apply efficiency corrections and to perform systematics studies.

- Use of python scripts results in highly automated and reproducible job control. The entire analysis code and all efficiencies and reweighting parameterizations are in CVS. Version tracking is employed. Every CAFe log file contains the full CAFe configuration file content and a full CVS diff output for all packages.

- Standard software packages are used whereever possible. The list of packages with version numbers used in this analysis is given in Appendix A

Integrated luminosity information from the luminosity system is *not* used; but relative instantaneously luminosity measurements *are* used to make luminosity-dependent efficiency corrections. To "blind" the analysis to the true value of the integrated luminosity, an unknown-to-the-analyzers number of additional luminosity blocks have been removed from the data set. The blinding fraction is different for each data sample described in Table 1, thus also blinding time dependence of the cross section measurement.

2 Data Selection

Event selection for this analysis mainly follows Ref. 1 in that we select events with two isolated muons, with a muon identified by requiring a central detector track reconstructed in 3-D that is matched to a muon chamber track of at least "loose" quality. A significant difference is that here is no η restriction on muons. Muons from the bottom hole of the muon system are included in the analysis. Muons with a z coordinate at their *dca* outside of ± 40 cm are rejected to ensure good silicon tracker efficiency for selected tracks.

The Z yield is extracted separately for a relatively large number of run periods that correspond to changes in detector configuration that could result in significant acceptance and efficiency modifications. Towards the aim of providing a cross check of the luminosity monitor, further subdivisions of the run 2A data sample are introduced due to modifications to the DØ luminosity monitor readout. These periods are summarized in Table 1.

Runs declared as having bad data quality according to the Calorimeter, SMT, CFT and Muon groups are removed. Runs with trigger list versions 13 and 14 where the L1 track trigger monitoring crate (0x13) was not included in the readout are not used in the analysis. The information delivered by this crate is needed to match offline tracks to trigger objects. Runs for which no precise beam spot parameterization is available are rejected because beam spot information is used to constrain the momentum of tracks without silicon detector hits. Luminosity blocks declared as bad for any specific trigger used in the analysis are similarly removed. Luminosity blocks declared bad by the luminosity system itself are also rejected. Data period v13b does not contain any events passing the data quality selection and is therefore not analyzed.

Runs with test trigger lists during the transition to a new major trigger list version are excluded from the data samples. This affects triggers lists 12.00-12.02, 14.00, and the first four runs of version 11.00.

3 Event Selection Cuts: $Z \to \mu^+\mu^-$ signal sample

Event selection requires evidence that a pair of oppositely charged, high p_t muons is produced. The muons are identified by requiring a track in the central detector that is matched to a track of at least "loose" quality[3] in the muon chambers. In order to reduce the background from muon pairs in $b\bar{b}$ events, the two muons are required to pass the "two out of four" isolation crieria given below; this maintains a very high efficiency to be retained for $Z \to \mu^+\mu^-$ events containing jets. In order to reduce the background from cosmic ray muons traversing the detector, cuts are made on the times measured by the muon scintillators and on the *dca* of the muon tracks.

For tracks that only have hits in the CFT, $\frac{q}{p_t}$ (charge over transverse momentum) is corrected by introducing a constraint to the average beam spot location derived from beam position and beam slope parameters for each run as provided by G. Borrisov. Only *dca* and p_t are calculated, using the following formula [4]:

$$\left(\frac{q}{p_t}\right)' = \frac{q}{p_t} - \left(\frac{\sigma_{dca,\frac{q}{p_t}}}{\sigma_{\frac{q}{p_t},\frac{q}{p_t}}} \times dca\right), \tag{2}$$

Run Start (r)	**Run Stop** (r')	**Version**	**Beginning of dataset comment**
160582	167015	v8	Trigger list change
167019	170246	v9	Trigger list change
170247	174802	v10	Trigger list change
174896	178721	v11	Trigger list change
178722	180956	v12a	Trigger list change
184951	190370	v12b	Oct. 2003 shutdown
191266	194597	v12c	Mar. 2004 shutdown
194567	196584	v13a	Trigger list change
201485	201936	v13b	Aug. 2004 shutdown, sol. change
202152	204805	v13c	Lumi. electronics change
204807	206161	v13d	2nd Lumi. electronics change
206162	208144	v13e	VME available in Lumi.
207728	211213	v14a	Trigger list change
211214	212107	v14b	VME primary in Lumi.
212804	215670	v14c	Nov. 2005 shutdown

Table 1: Summary of data sub-sets.

where *dca* is the distance of closest approach of the muon track to an approximation of the beam spot position in the $r-\phi$ plane, and $\sigma_{dca,\frac{q}{p_t}}$ and $\sigma_{\frac{q}{p_t},\frac{q}{p_t}}$ are the $\left(dca, \frac{q}{p_t}\right)$ and $\left(\frac{q}{p_t}, \frac{q}{p_t}\right)$ elements of the track fit covariance matrix, respectively. The formula describes the change in $\frac{q}{p_t}$ that is expected from the relevant track parameter covariance matrix elements if the impact parameter is changed from its original value *dca* to its new value 0 (both with respect to the average beam spot).

Having required two central detector tracks matched to at least "loose" quality muons, the following cuts are applied:

1. The projections of both muon tracks are required to lie within the geometrical acceptance of the muon chambers.

2. $p_t > 20$ GeV for both muons, where p_t is the momentum of the matched central detector track measured in the plane transverse to the $p\bar{p}$ beam direction. This tightens the $p_t > 15$ GeV cut used in Ref. 1 and aligns the event selection cuts with those used for trigger efficiency studies.

3. $70 < M_{\mu\mu} < 110$ GeV/c^2, where $M_{\mu\mu}$ is the dimuon invariant mass.

4. The two muons must satisfy between them two of the four possible isolation criteria below, in any combination:

   (a) $\Sigma_{cone0.5}(p_t) < 2.5$ GeV, where $\Sigma_{cone0.5}(p_t)$ is the sum of p_t of tracks contained within a cone around the muon of width $\Delta R < 0.5$.

   (b) $\Sigma_{halo}(E_t) = \Sigma_{cone0.4}(E_t) - \Sigma_{cone0.1}(E_t) < 2.5$ GeV, where $\Sigma_{cone0.1}(E_t)$ and $\Sigma_{cone0.4}(E_t)$ are sums of the E_t of calorimeter clusters in cones around the muon of widths

$\Delta R < 0.1$ and $\Delta R < 0.4$, respectively. In forming these sums, cells in the electromagnetic and fine hadronic calorimeters are considered, but not those in the coarse hadronic calorimeter.

5. The muons are required to be oppositely charged.

6. $|\Delta t| < 10$ ns for each of the two muons, where Δt is the arrival time of the muon with respect to the bunch crossing, adjusted for flight time to the muon system.

7. $dca < 0.2$ cm for for muon track with no SMT hits, and $dca < 0.02$ cm for tracks with at least one SMT hit.

8. The difference of z coordinates of the two muons at dca, Δz, is required to be less than 3 cm.

9. Cosmic muons tend to be reconstructed as two exactly back-to-back muons. To suppress this kind of background, muons are required to be acolinear by cutting on pseudo-acolinearity $\Delta\alpha_{\mu\mu} = |\Delta\phi_{\mu\mu} + \Delta\Theta_{\mu\mu} - 2\pi| > 0.05$.

10. Candidate events are required to have fired one of the triggers summarized in Table 4. The central values for yields are taken from the italicized trigger in each epoch. The (overlapping) event selections triggered on by each other trigger are used to cross check the trigger efficiency measurements.

Note that event selection closely follows Ref. 1, with these exceptions:

- The dimuon invariant mass is restricted from $70 - 110$ GeV/c^2 to allow comparison to an ongoing electron analysis.

- The muon p_T cut has been raised to 20 GeV for consistency with the muon sample used in the muon identification and trigger efficiency measurements certified by the muon ID group. The motivation for this is that many triggers have a 15 GeV muon momentum requirement, and the 20 GeV cut is chosen to minimize any turn-on effects in the efficiency determination.

- A cosmic ray timing cut of ± 10 ns has been imposed. Although there are other possibilities to reduce cosmic muon background to acceptable levels in dimuon events, this cut was included in anticipation of a future $W \to \mu\nu$ cross section analysis with muon selection as similar as possible to the current $Z \to \mu\mu$ analysis in order to minimize systematic uncertainties of a cross section ratio measurement.

Trigger efficiencies and reconstruction efficiencies of muon objects and central tracks are measured in data and applied as corrections to Monte Carlo simulated events with full GEANT detector simulation. Selection cut efficiencies on quantities that are modeled well in the simulation are taken from Monte Carlo; cuts on quantities that are not well described are corrected with measurements in data. Most background contributions are also estimated from actual data, as described in the subsequent section.

4 Background evaluation

This analysis employs very tight selection cuts to reduce background to the sub-percent level. Noticeable background contributions are, in decreasing order of importance,

- W **in events with an extra high** p_t **muon, faking Z candidates:** this contribution is mainly reduced by tight Z mass and muon p_t cuts.
- **QCD background (mainly** $b\bar{b}$**):** large p_t cuts and isolation requirements on the muons suppress most of this background.
- **cosmic muons:** cosmic background is diminished by acolinearity requirements on the two muon candidates, plus scintillator timing cuts
- $Z \to \tau\tau$ **decays misidentified as** $Z \to \mu\mu$**:** a high minimum Z mass requirement helps reduce this contribution.

$Z \to \tau\tau$ background is evaluated using Monte Carlo simulated events. All other contributions are measured in data. The background level is too low to allow a precise evaluation on the individual subsamples described in Section 1. Therefore the background levels are measured on the combined dataset, and measurements on individual subsets are only used to check for any time dependence beyond statistical uncertainties.

Another contribution to the sample of selected events that is treated as background is the contribution of dimuon pairs with reconstructed invariant mass in the 70-110 GeV/c^2 mass window that originates from γ/Z with true invariant masses outside the 60–130 GeV/c^2 mass range that we normalize our measurement to. This contribution is estimated using Monte Carlo simulated events as described below and subtracted from the number of selected events in data.

The abovementioned background contributions will be discussed in the following parts of this section. The QCD background evaluation will be introduced in Section 5.1 as part of a detailed study of isolation and charge cut efficiency.

4.1 W plus muon background

The rate of events with $W \to \mu\nu$ decays and an additional muon that together pass all $Z \to \mu\mu$ selection cuts is evaluated by looking at the rate of events with a $Z \to \mu\mu$ decay and an additional muon such that at least two Z candidates passing all cuts are found in the same event. The fraction of events with extra Z candidates is scaled up by the ratio of the W and Z production cross sections times branching fraction into muon(s). This ratio was measured to be 10.94. As a result, the background fraction is estimated to be (0.11±0.05)%, where the uncertainty is statistical.

4.2 Cosmic muon background

A large fraction of cosmic muons traversing the detector is removed by the cut on distance of closest approach of the muon tracks to the interaction region. A pseudo-acolinearity cut is used to remove exactly back-to-back muons that are more likely to originate from cosmic

true $\gamma/Z \to \tau\tau$ invariant mass	**relative background contribution**	
	before 2004 shutdown	**after 2004 shutdown**
15–60 GeV/c^2	0.0%	0.0%
60–130 GeV/c^2	81.3%	81.5%
130–250 GeV/c^2	17.4%	17.1%
250–500 GeV/c^2	1.3%	1.4%
500–1000 GeV/c^2	0.0%	0.0%

Table 2: Fraction of contribution to overall $\gamma/Z \to \tau\tau$ background of different γ/Z invariant mass ranges. The composition is different for datasets v08-v13a (before the Tevatron fall 2004 shutdown) and v13b-v14c (after the 2004 shutdown) due to changes in the muon momentum resolution.

muons traversing the detector. Most of the remaining cosmic muon background is removed by a ± 10 ns cut on the time of muon scintillator hits associated with the candidate muons, measured relative to the time the beam interaction took place and corrected for muon flight time from interaction region to muon detectors.

The remaining fraction of cosmic muons in the event is estimated from the time difference of scintillator hits associated with both Z candidate muons. For actual $Z \to \mu\mu$ events this time difference is expected to be close to zero, whereas cosmic muons should exhibit a significant time difference due to their crossing the detector at light speed c. The contributions can thus be distinguished by calculating the apparent speed needed to cause scintillators hits at the measured times, assuming they were caused by a cosmic muon. Cosmic muons should cluster at c, whereas muon pairs from Z decays are expected to have infinite apparent speed. Due to limited time resolution, the apparent speed of $Z \to \mu\mu$ decays constitutes a broad distribution with a tail that extends down to c and lower. We therefore estimate the cosmic background contribution to be half of the fraction of events with apparent speed of c or lower, i.e. 0.03%, and assign a 100% relative uncertainty to this background measurement.

4.3 $Z \to \tau\tau$ background

The fraction of $Z \to \tau\tau$ events faking $Z \to \mu\mu$ events in the sample of selected Z candidates is evaluated using $\gamma/Z \to \tau\tau$ Pythia Monte Carlo samples with γ/Z invariant mass range 15-1000 GeV/c^2, processed with the same full GEANT simulation of the DØ detector as the $Z \to \mu\mu$ Monte Carlo used in this analysis. This fraction is measured to be 0.04% for data periods v08–v13a, with a relative statistical uncertainty of about 3%. Due to decreased track momentum resolution, in part due to a reduction in solenoid current, an increased $Z \to \tau\tau$ background fraction of 0.05% is expected for data periods v13b-v14c. The contribution of different $\gamma/Z \to \tau\tau$ mass bins to the overall fraction is shown in Table 2. The numbers given in the table are averages over all subsamples. They are evaluated separately for each subsample in the analysis to account for small variations due to different triggers and time dependent detector performance.

true $\gamma/Z \to \mu\mu$ invariant mass	**relative contribution**	
	before 2004 shutdown	**after 2004 shutdown**
15–60 GeV/c^2	0.1%	0.1%
60–130 GeV/c^2	99.9%	99.9%
130–250 GeV/c^2	0.0%	0.0%
250–500 GeV/c^2	0.0%	0.0%
500–1000 GeV/c^2	0.0%	0.0%

Table 3: Fraction of contribution to overall $\gamma/Z \to \mu\mu$ event selection from different γ/Z invariant mass ranges, before and after the Tevatron shutdown in fall 2004

4.4 $\gamma/Z \to \mu\mu$ events outside the 60-130 GeV/c^2 mass window

The intention of this note is to quote a yield of $\gamma/Z \to \mu\mu$ events with γ/Z invariant masses between 60 and 130 GeV/c^2. Thus we need to predict the relative size of the contributions from within and without this mass window to the sample of selected events in data, and subtract the latter fraction as background. The fraction of selected events in the reconstructed mass window originating from several mass bins in the range 15–1000 GeV/c^2 is determined using Pythia Monte Carlo with full GEANT detector simulation. Like $Z \to \tau\tau$ background, the overall scale as well as the contributions from the individual mass bins is evaluated separately for each data period. Table 3 shows average values of the relative contributions.

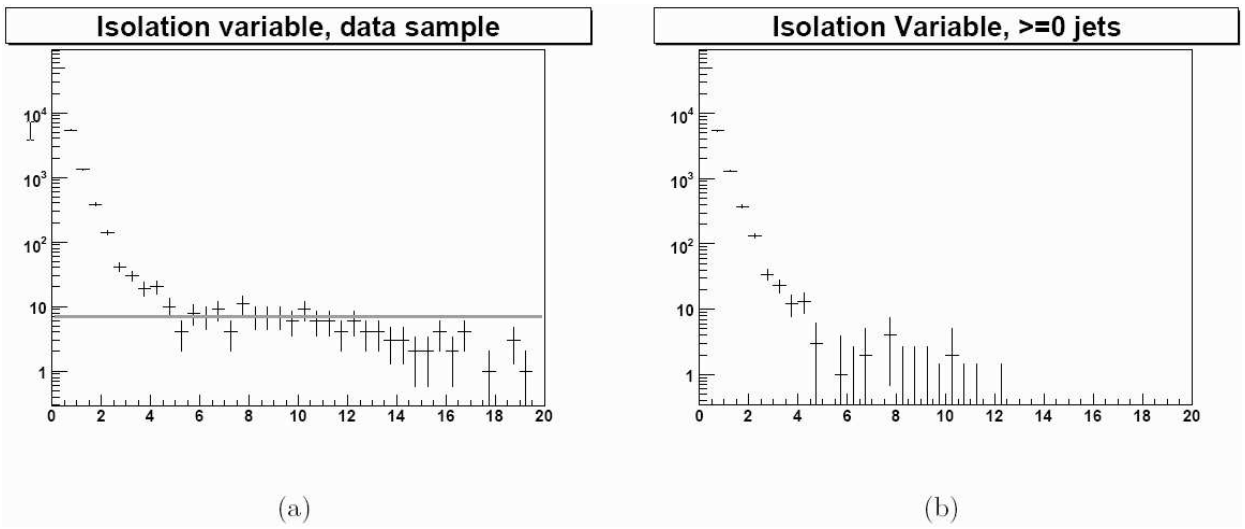

Figure 1: The second smallest isolation variable in each event passing all cuts, without applying the isolation cut. (a) The distribution of all events, and the line used to extrapolate the QCD background into the signal region. (b) The distribution after subtracting the fitted line.

5 Isolation Efficiency, Charge Cut Efficiency and QCD Background

The main cut used to reject QCD (semi-leptonic heavy flavour decays) is the isolation cut. There are two things we need to know for this analysis: how many QCD events remain after applying the cut, and how many signal events are rejected by the cut. This section will also cover a related quantity, the efficiency of the opposite charge requirement. Note that for these studies, a large data sample is used to increase statistics. It is assumed that the values derived in this section are the same for all data subsets. More details are available in DØ Note 5177[5].

5.1 QCD Background

In order to study the effect of the isolation cut, we must first simplify the definition slightly. The cut applied requires that any two out of four isolation requirements pass, when the calorimeter halo is required to be below 2.5 GeV, and the track halo below 3.5 GeV. The first simplification is to scale the track isolation by $2.5/3.5 = 0.714$, meaning all criteria are now required to be below 2.5 GeV. Then, taking the four isolation requirements in each di-muon event (scaled track halo on each muon, calorimeter halo on each muon) and placing in order of increasing size, we only really require that the second smallest be below 2.5 GeV, as we allow two variables to fail this cut. Thus, when studying the effect of this isolation cut, we only need to look at the second smallest isolation variable in each event. Plotting this variable for events which pass all other cuts shows (Fig. 1) the distribution of signal (at low values) and QCD background (at higher values).

To further understand this distribution Fig. 2 compares the isolation variable distribution from Monte Carlo samples of QCD $b\bar{b}$ and $Z \to \mu\mu$ events to what is seen in the data. This $b\bar{b}$ Monte Carlo is an inclusive sample of decays to muons, pre-selected to contain at least one muon with p_T above 8 GeV. In order to retain sufficient statistics, only *one* muon is required, with p_T above *10* GeV. Then the highest isolation variable for this muon is plotted. This would allow a second muon in the event to be non-isolated, and the event would still pass the 2/4 isolation cut. Finally, we can look in data at the mass range $40 - 60$ GeV, where we expect more background and less signal. The distribution of these events is also shown in Fig. 2. Returning to the signal data sample, and the method used to estimate the QCD background in the signal region. We fit the QCD distribution in a region that is largely signal free ($5 - 10$ GeV), and extrapolate into the signal region (below 2.5 GeV), A flat line is used to model the QCD distribution. It can be seen that the actual distribution drops at higher values of the isolation variable, and it is expected to drop at lower values in the signal region, as seen in the Monte Carlo. So this method provides a slight over-estimate of the QCD background. The fitted line is subtracted from the data, and the remaining distribution can be compared to $Z \to \mu\mu$ Pythia Monte Carlo.

This method gives an estimate of 35 QCD events in the signal region (below 2.5 GeV), which contains a total of 56194 events. While this is expected to be an over-estimate of the background, we apply a 50% uncertainty to cover any variations in the QCD distribution, along with the statistical uncertainty. The QCD background is thus $0.06 \pm 0.03\%$ of the sample. The previous analysis found a QCD background of 0.5%, however this analysis uses higher p_T cuts (20 vs. 15 GeV) and a much narrower mass window ($70-110$ GeV vs $40-\infty$). As the QCD background is concentrated at low p_T and low mass, this analysis expects to have a significantly lower QCD background. Repeating the method with the cuts used in the old analysis ($p_T > 15$ GeV, mass > 40 GeV) gives the distribution shown in Fig. 3, and a QCD estimate of $0.6 \pm 0.3\%$.

5.2 Isolation Cut Efficiency

In Fig. 1 it can be seen that there is an excess over the expected QCD background when the isolation variable is below 6 GeV. This excess in the region $2.5 - 8.0$ GeV is attributed to $Z \to \mu\mu$ signal events which fail the isolation cut, and so can be used to measure the isolation cut efficiency. Before subtracting the QCD background, there are a total of 163 events in the region $2.5 - 8.0$ GeV GeV. After subtracting, there remain 88 events. As we are expecting the QCD background to be over-estimated, we assume the true number of rejected Z events lies between 88 and 163, so we quote the mid point and take the difference as a systematic. Thus the number of signal events failing the isolation cut is $125.5 \pm 11.2(\text{stat.}) \pm 37.5(\text{syst.})$, which corresponds to a cut efficiency of $99.78 \pm 0.07\%$, after applying all other cuts. In the Pythia sample, this cut efficiency is found to be 99.77%.

5.3 Opposite Charge Selection Efficiency

Figure 4 shows the distribution of the isolation variable for like sign events. Any Z events with a mis-identified muon charge will appear at low values, and indeed there is an excess there. To provide an estimate of this excess, the method used on the unlike sample is used

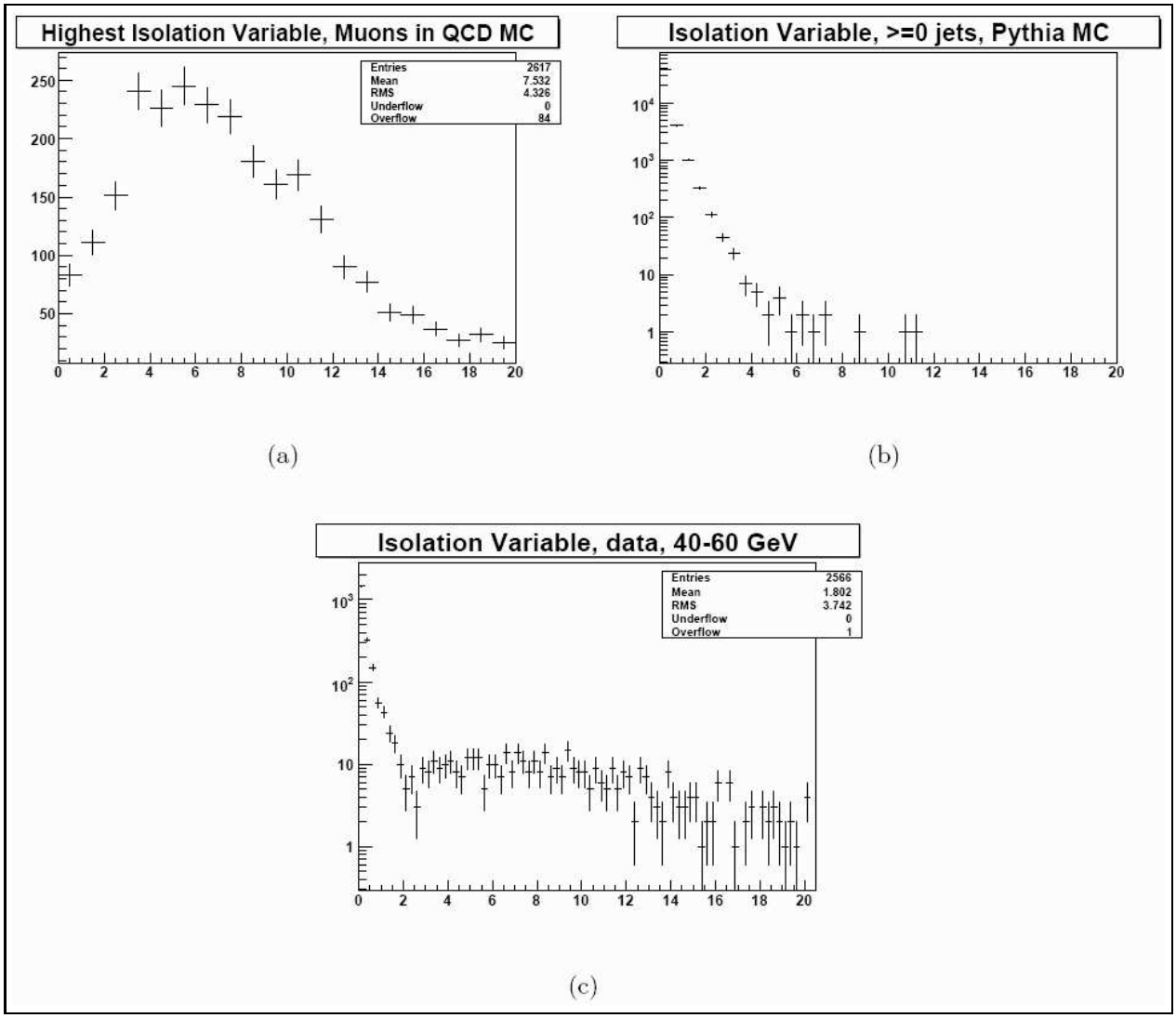

Figure 2: (a) The highest isolation variable for muons in the QCD $b\bar{b}$ Monte Carlo sample. The second smallest isolation variable in each event passing all other cuts in (b) Pythia $Z \to \mu\mu$ Monte Carlo and (c) data in the mass region $40 - 60$ GeV.

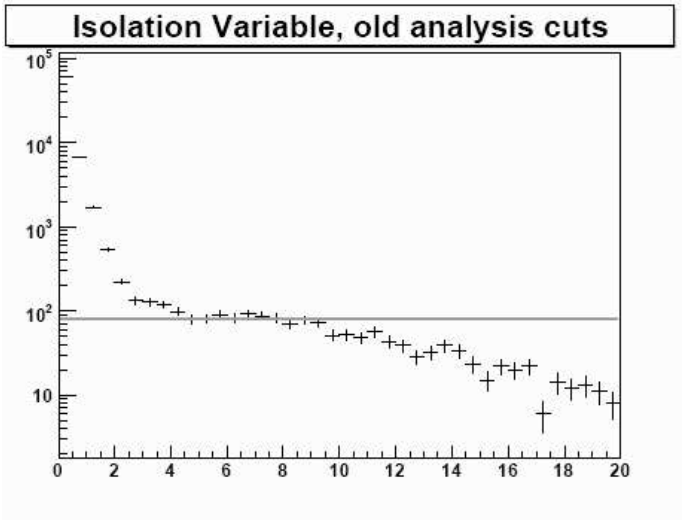

Figure 3: The isolation variable with the cuts used in the previous analysis ($p_T > 15$ GeV, mass > 40 GeV).

again. Fitting the QCD distribution with a flat line in the region $5 - 10$ GeV and extrapolating in to the signal region (below 2.5 GeV) gives an estmated background contribution of 4.2 events to the 40 events found in the signal region. Again, assuming this is actually an overestimate of the QCD background, we assume the background is actually half this value, and quote the difference as a syatematic. The number of signal events failing the charge cut is thus $37.9 \pm 6.2(\text{stat.}) \pm 2.1(\text{syst.})$. This corresponds to a charge cut efficiency of $99.94 \pm 0.01\%$. In Pythia Monte Carlo, we find a charge mis-id rate of 99.98%. The previous analysis found a larger charge cut inefficiency of 0.2%. However, as track which have mis-measured charges also have mis-measured p_T, we expect many of these events would not fall inside the tighter mass window of this analysis. Thus we expect a significantly lower charge mis-id rate.

5.4 Summary

We measure a QCD background of $0.06 \pm 0.03\%$, the isolation cut efficiency for signal to be $99.78 \pm 0.07\%$, and the opposite charge requirement for signal to be $99.94 \pm 0.01\%$. These values were measured on a large dataset, and are assumed to be the same for each of the subsets studied.

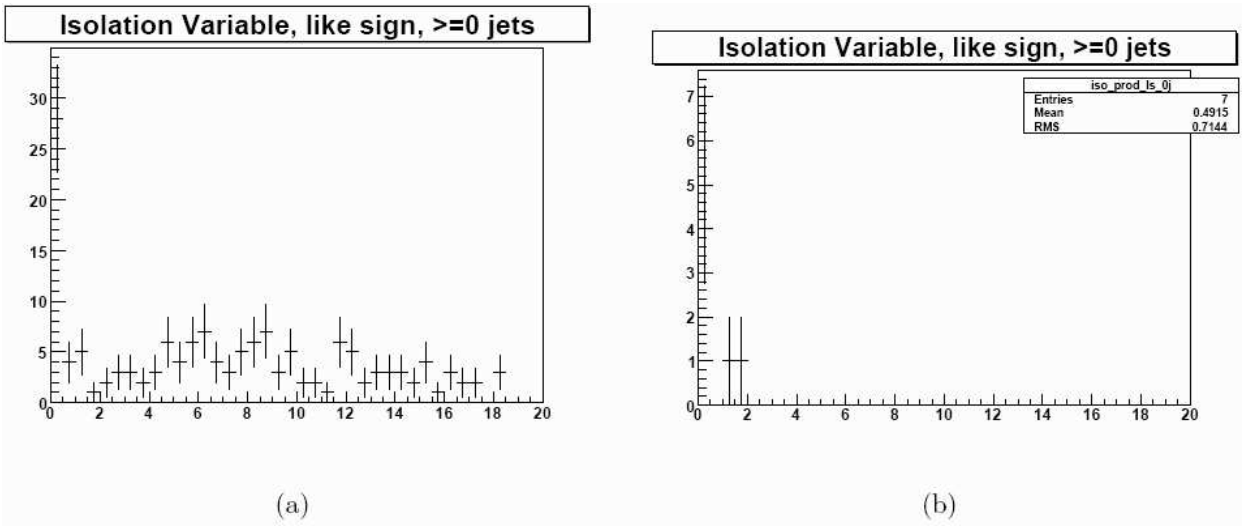

Figure 4: The second smallest isolation variable in like-sign events passing all other cuts, without applying the isolation cut. (a) The distribution in data, where all entries below 2.5 GeV are attributed to mis-identified $Z \to \mu\mu$ events. (b) The distribution in a Pythia Monte Carlo.

6 Trigger, Reconstruction, and Matching Efficiencies

Efficiencies for trigger+reconstruction+matching are evaluated using the data following the tag and probe method. Efficiency corrections are then implemented for the MC. There is a fundamental difference between tracking/muonID efficiencies and trigger efficiencies that comes from the fact that we are using full GEANT MC. This MC already includes reasonably well modelled tracking and muonID efficiencies. These are corrected by the ratio of tag and probe efficiencies measured by muo_cert for data and MC. This approach is considered very safe and reliable because correlations like muons disappearing in cracks on opposite sides of the detector (an inefficiency that is invisible to simple tag and probe) will be fairly well taken care of by the MC itself.

We have made the judgement that the analogous trigger simulation tool `trigsim` is not yet sufficiently mature for this analysis. Therefore we implement trigger efficiencies directly through absolute measurement and cross check our results with as many different triggers as possible. We expect that any biases in our trigger efficiency measurement can be identified by comparing yield measurements for the same data sample, obtained with different number (single muon triggers versus dimuon triggers) and type (e.g. track triggers versus muon system triggers) of measured efficiencies. Studies involving `trigsim` software have been prepared (`trigsim`-capable MC samples are available), but will be done at a later stage.

For tracking efficiency, we require a local muon for the probe and then look for a track. For triggers, things are done the same way as for offline muonID or tracking efficiencies, depending on whether we are measuring the efficiency of a muon system trigger or a track trigger. The selection cuts for the tag muon are tighter than the one used for Z selection in order to keep background contamination (with associated risk of bias) low. The probe muons have to pass the same selection cuts as the muons used in the analysis.

Muon and tracking systems are treated as uncorrelated in this analysis. Obviously there is a physical correlation between signals in the two detector systems, but it is fully absorbed by the fact that we are requiring track matched local muons and measure all efficiencies relative to that assumption.

The wzreco/muo_cert package is used to determine tag and probe efficiencies of individual trigger objects such as specific L1 muon terms, L1 CTT tracks, L2 muon objects, L3 muon objects or tracks. At this stage the analysis results are based on selection of a single trigger. No XORing or explicit ORing operations are performed. For example, the yield for trigger MUH1_TK12_TLM12 is extracted from events which fire this trigger, independent of the status of any other trigger. The variation of results with trigger condition is used as a check.

Muo_cert calculates efficiencies assuming specific matching conditions between offline muons and trigger objects. Offline tracking and muon ID corrections are applied to MC samples with CAF processor `MuonCorr` from the `caf_eff_utils` package. A new CAF processor `MuonTriggerMatch` has been written to impose corresponding matching conditions in data selection; and a second new CAF processor `Probability_nMuon` has been written to calculate trigger probabilities accordingly. Both processors have been made available to all DØ physics groups as part of the `caf_trigger` package and have been tested in other analysis projects as well.

All efficiencies are parameterized for MC corrections as functions of pairs of the most

Epoch	Dimuon	Single Muon
v08–v09	*2MU_A_L2M0* mu2ptxatxx_fz	
v10	*2MU_A_L2M0*	MUW_W_L2M3_TRK10
v11	2MU_A_L2M0 2MU_A_L2M0_TRK10	*MUW_W_L2M3_TRK10*
v12a–v12c	2MU_A_L2M0 2MU_A_L2M0_TRK5	*MUW_W_L2M3_TRK10*
v13a	*DMU1_LM6* DMU1_TK5	MUH1_LM15 MUH2_LM15 MUH1_TK12
v13c–v13e	DMU1_TK8 DMU1_LM15	*MUH1_TK12_TLM12* MUH1_LM15
v14a–v14c	DMU1_2LM6 DMU1_LM6_TK12 DMU1_TK8_TLM8	*MUH1_TK12_TLM12* MUH1_ILM15

Table 4: Di-muon and single muon triggers used in this analysis. The italicized triggers are used for the final yield determinations. The others are used for cross checks.

relevant kinematic quantities as follows:

- For offline/L1/L2/L3 muon identification, efficiency is binned in ϕ and muon detector η.
- For offline L3 tracking, efficiency is binned in vertex z and CFT detector η.
- For L1CTT efficiency, the binning is in ϕ and CFT detector η.
- For the L3 muon_cm tool track matching efficiency, binning is in ϕ and muon detector η.

Correction weights are applied to all MC muons passing all selection cuts required in this analysis. Muon and track reconstruction efficiency correction weights are multiplied for each such muon in the event to get an overall event correction weight. Trigger efficiencies are treated as described in Section 6.1. Statistical uncertainties of the binned efficiency corrections are propagated assuming Gaussian uncertainties in each bin, and properly taking correlations between different events due to correction weights taken from the same bins into account.

6.1 Trigger efficiency calculation

The trigger efficiency measurement is based on the probability that a given offline reconstructed and track matched muon fires specific trigger objects. The `Probability_nMuon` processor distinguishes up to two trigger conditions built from these trigger objects. For example, the v13 dimuon trigger DMU1_LM6 requires two L1 muon l1atxx objects, one

medium quality L2 muon l2m0 and one >6 GeV loose quality L3 local muon l3l6. This is translated into the two trigger conditions

condition 0: l1atxx AND l2m0 AND l3l6

condition 1: l1atxx

The probability to fire either of the trigger conditions is a product of the individual term probabilities. These probabilties are calculated for each muon in the event passing all muon selection cuts. The trigger event probability is then derived from all combinations of muons and their associated probability of firing either of the trigger conditions. Single muon triggers are modeled by always assigning probability 1 to the second condition.

The trigger probability calculation assumes specific matching conditions between offline reconstructed muons and trigger conditions. In the example above, a case where one muon fires L1 and L2 but not L3, and the other muon fires L1 and L3 but not L2 would not be counted as efficient. Correspondingly, events with such configurations are rejected by the `MuonTriggerMatch` processor in data, even if the trigger we are interested in did fire. These strong matching requirements can lower the apparent trigger efficiency significantly with respect to the trigger efficiency evaluated without any matching criteria. It is therefore not easily possible to compare trigger efficiencies quoted in this document with earlier results. Instead, we cross check both the trigger term efficiency measurements and the combination thereof into event probabilities by comparing the measured yields obtained with data selection and efficiency measurements for different triggers on identical datasets.

All efficiencies are measured separately for each data period in Table 1, with the exception of periods v08-v10 which lack sufficient numbers of Z candidates to measure efficiencies binned in two dimensions with adequate granularity. Here we use efficiencies measured on the combination of the v08-v11 samples instead.

7 Determination of Y_Z

The yield for any data taking epoch follows from the expression:

$$Y_Z = \frac{N_{\rm cand}(1 - f_{backgr} - f_{massbins})}{\epsilon_{Z\gamma}}, \tag{3}$$

with $N_{\rm cand}$ the number of selected events, f_{backgr} is the fractional background as described in Sections 4 and 5, $f_{massbins}$ is the contribution from signal events with true γ/Z mass outside the 60–130 GeV/c^2 mass range, and $\epsilon_{Z\gamma}$ is the total efficiency for $p\bar{p} \to Z/\gamma^* \to \mu^+\mu^-$.

The total efficiency $\epsilon_{Z\gamma}$ is evaluated according to

$$\epsilon_{Z\gamma} = \epsilon^{\rm eff}_{\rm MC} \times \epsilon_q \times \epsilon_{\rm isol} \times \epsilon_{\rm cosmic} \times \epsilon_{\rm DQ} \times \epsilon_{{\rm fast}Z} \times \epsilon_{L3{\rm match}} \times \epsilon_{\rm pre} \tag{4}$$

where

- $\epsilon^{\rm eff}_{\rm MC}$ takes into account the geometrical acceptance of the muon chambers and the efficiency of the "kinematic" cuts on p_t and $M_{\mu\mu}$. It includes a number of data-to-Monte Carlo corrections measured using the tag and probe technique for the trigger ($\epsilon_{\rm trig}$), tracking ($\epsilon_{\mu{\rm trk}}$), and loose muon identification efficiencies ($\epsilon_{\mu{\rm ID}}$). Re-weighting factors are also applied for the instantaneous luminosity profile ($\epsilon_{\rm lumi}$), actual vs. nominal beam shape ($\epsilon_{\rm beam}$), the NLO cross section reweight ($\epsilon_{\rm NLO}$), and a possible PDF reweight ($\epsilon_{\rm PDF}$). The various terms are described more fully below and in a separate section on efficiencies.

- ϵ_q is a correction factor for the slightly different efficiencies of the opposite charge requirement in data and in Monte Carlo, which is taken to be a constant $\epsilon_{\rm opposite\_q} = (99.94 \pm 0.01\%)/99.98\%$ for all epochs, as described in Sec. 5.3.

- $\epsilon_{\rm isol}$ is a correction factor for the slightly different isolation cut efficiencies in data and Monte Carlo, taken to be a constant $\epsilon_{\rm isol} = (99.78 \pm 0.07\%)/(99.77\%)$ as described in Sec. 5.1.

- $\epsilon_{\rm cosmic}$ is a correction factor for the different cosmic ray timing cut efficiencies in data and Monte Carlo due to unrealistic modeling of the timing resolution. This is measured separately for each dataset, varying between 96.7% and 101.4% due to different calibrations. It is applied as an overall correction factor.

- $\epsilon_{\rm DQ}$ is the fraction of events passing the calorimeter event quality selection. This is determined for each epoch and applied as an overall correction factor. It is measured on a sample of $Z \to \mu\mu$ candidates passing all selection requirements except the isolation cut. Without the isolation cut, the Z candidate selection is independent of the DØ calorimeter, and therefore allows an unbiased determination of the calorimeter event data quality flag efficiency.

- $\epsilon_{{\rm fast}Z}$ is the efficiency of the level 0 fast Z requirement, operational only for epochs before v10 and for a part of epoch v10 itself. The efficiency of this trigger requirement was determined to be 94.3% in Ref. [1]. For v10, we assign a fastZ efficiency of (94.3% +

100%)/2 and assign the full range between 94.3% and 100% as systematic uncertainty because we cannot obtain an integrated luminosity weighted average efficiency in this analysis. This is applied as an overall correction factor. It is unity for epochs v11 and later.

- $\epsilon_{L3\text{match}}$ is a level 3 track matching efficiency only needed for epochs v13a–v13e. The MUH1_TK12_TLM12 trigger used in v13 and v14 samples makes use of L3 matching code the efficiency of which can be measured with muo_cert in v14 only. v13 data do not contain the necessary information for muo_cert to determine this term, and therefore we measure an overall correction factor it with separate code. The procedure is to tag events triggered by MUH1_LM15, which has the same L1 and L2 requirements as MUH1_TK12_TLM12. In these events, we also require a 12 GeV L3 track that is matched to the same offline muon that is also matched to the 15 GeV local muon the trigger fired on. The fraction of events fullfilling these conditions and also firing MUH1_TK12_TLM12 is the L3 matching efficiency. We cross check this method by comparing its result in v14 (using MUH1_ILM15) with the muo_cert measurement of the matching efficiency and find good agreement.

- ϵ_{pre} is the trigger prescale correction. This is determined separate for each epoch and applied as an overall correction factor. In analyses using integrated luminosity information, the effect of prescaled triggers is included in the luminosity determination for a specific trigger: a trigger with prescale factor 2 on the same sample as another trigger with prescale factor 1 is defined to have half the integrated luminosity. That way the effect of prescales cancels in the cross section calculation. Since we cannot use integrated luminosity, but still want to compare yields measured with different triggers (and different prescales), we correct for prescale effects by determining a prescale efficiency. For each event selected in data with a prescale P, we count P events in a sum of events that results into the number of selected events we would have expected if the trigger never was prescaled. The ratio of the actual number of selected events and the prescale weighted sum is the prescale correction, or fraction of events surviving prescaling.

Tables 5 and 6 detail the calculation of $\epsilon_{\text{MC}}^{\text{eff}}$ for the trigger epochs.

7.1 Monte Carlo: the factor $\epsilon_{\text{MC}}^{\text{eff}}$

The factor $\epsilon_{\text{MC}}^{\text{eff}}$ begins with the full version `p17.09.01` (v08-v13a) or `p17.09.06` (v13c-v14c) GEANT MC with extra muon resolution smearing using the PYTHIA event generator[10] with the CTEQ6L1 parton distribution function (PDF) and a generator level mass cut of 60 GeV/$c^2 < M_{\mu\mu} <$ 130 GeV/c^2. The invariant mass range is extended to 15–1000 GeV/c^2 using `p17.09.01` Monte Carlo.

As is well known, the full GEANT Monte Carlo predicts a mass resolution at the Z^0 peak that is narrower than that observed in the data. The procedure to correct for this follows several other analyses and applies extra Gaussian smearing to $\frac{q}{p_t}$ in order to achieve agreement between data and MC in the width of the Z. The amount of smearing varies as

correction	**v08**	**v09**	**v10**	**v11**	**v12a**	**v12b**	**v12c**
uncorrected $\epsilon_{\rm MC}^{\rm nom}(\%)$	35.49	35.49	35.49	35.49	35.49	35.49	35.49
muon ID	0.9581	0.9584	0.9600	0.9626	0.9297	0.9838	0.9906
muon tracking	0.9687	0.9684	0.9685	0.9728	0.9664	0.9416	0.9449
trigger	0.6323	0.6323	0.6323	0.7634	0.7579	0.7874	0.7691
luminosity profile	1.1577	1.0885	1.0416	1.0347	1.0195	1.0022	0.9987
beam shape	0.9058	0.9061	0.9072	0.9091	0.9090	0.9395	0.9751
NLO reweight	0.9956	0.9957	0.9952	0.9987	0.9985	0.9995	0.9993
Reweighted $\epsilon_{\rm MC}^{\rm eff}(\%)$	19.51	19.50	19.47	23.39	22.34	24.58	24.92
Cal. Data Quality	0.9892	0.9721	0.9704	0.9747	0.9661	0.9651	0.9589
Isolation Cut	1.0001	1.0001	1.0001	1.0001	1.0001	1.0001	1.0001
Charge Cut	0.9996	0.9996	0.9996	0.9996	0.9996	0.9996	0.9996
Timing Cut	0.9671	0.9858	1.0116	0.9953	0.9898	0.9898	1.0068
L1 Fast Z	0.9430	0.9430	0.9739	1.0000	1.0000	1.0000	1.0000
corrected $\epsilon_{\rm MC}^{\rm eff}(\%)$	0.1760	0.1762	0.1861	0.2268	0.2136	0.2347	0.2405
Pre-scale	1.0000	0.9972	0.9409	0.9907	1.0000	0.9985	0.9796
Candidates	202	1073	478	3529	2430	5195	5284

Table 5: Details of $\epsilon_{\rm MC}^{\rm eff}$ for trigger epochs v08-v12c. The first row of numbers contains the GEANT MC efficiencies without correction. This includes the geometric acceptance. The next rows contain multiplicative corrections extracted from the data using tag and probe techniques. The final rows contain the fully corrected efficiecies, applied pre-scale corrections and the number of Z candidates.

correction	**v13a**	**v13c**	**v13d**	**v13e**	**v14a**	**v14b**	**v14c**
uncorrected $\epsilon_{\rm MC}^{\rm nom}(\%)$	35.49	34.56	34.56	34.56	34.56	34.56	34.56
muon ID	0.9848	1.0012	1.0072	0.9901	1.0084	0.9626	1.0035
muon tracking	0.9503	0.9456	0.9423	0.9378	0.9191	0.8986	0.9056
trigger	0.6188	0.6430	0.6924	0.6826	0.7208	0.6897	0.7259
luminosity profile	1.0006	0.9986	0.9973	0.9984	0.9980	0.9948	0.9926
beam shape	0.9789	0.9865	0.9730	0.9848	0.9852	1.0060	0.9966
NLO reweight	0.9973	0.9985	0.9981	0.9986	0.9982	0.9982	0.9988
Reweighted $\epsilon_{\rm MC}^{\rm eff}(\%)$	19.92	20.55	21.92	21.49	22.75	20.91	22.65
Cal. Data Quality	0.9682	0.9685	0.9655	0.9657	0.9724	0.9488	0.9667
Isolation Cut	1.0001	1.0001	1.0001	1.0001	1.0001	1.0001	1.0001
Charge Cut	0.9996	0.9996	0.9996	0.9996	0.9996	0.9996	0.9996
Timing Cut	1.0073	1.0067	1.0010	1.0052	1.0057	1.0131	1.0138
corrected $\epsilon_{\rm MC}^{\rm eff}(\%)$	0.1942	0.1979	0.2092	0.2058	0.2224	0.2010	0.2219
Pre-scale	0.9892	0.9770	0.9948	1.0000	1.0000	1.0000	0.9791
Candidates	2570	5392	3651	5079	8918	3207	4594

Table 6: Details of $\epsilon_{\rm MC}^{\rm eff}$ for trigger epochs v13a-v14c. The first row of numbers contains the GEANT MC efficiencies without correction. This includes the geometric acceptance. The next rows contain multiplicative corrections extracted from the data using tag and probe techniques. The final rows contain the fully corrected efficiecies, applied pre-scale corrections and the number of Z candidates. Each column corresponds to the indicated trigger epoch.

a function of $\frac{q}{p_t}$. Both the absolute scale and the p_t dependence of the smearing are varied within their fit uncertainties to study the effect on theyield measurement.

$\epsilon^{\rm eff}_{\rm MC}$ then receives various data-to-MonteCarlo corrections measured through the tag and probe technique:

$$\epsilon^{\rm eff}_{\rm MC} = \epsilon^{\rm nom}_{\rm MC} \otimes \epsilon_{\mu\rm ID} \otimes \epsilon_{\mu\rm trk} \otimes \epsilon_{\rm trig} \otimes \epsilon_{\rm lumi} \otimes \epsilon_{\rm beam} \otimes \epsilon_{\rm NLO} \otimes \epsilon_{\rm PDF} \tag{5}$$

These are not a simple product of the trigger, kinematic and geometric terms; instead, the method used in its determination accounts for the correlations among the individual efficiency terms and correlations between the two muons. The symbol "$\otimes$" is used to denote this more complicated combination operation.

7.1.1 Nominal Monte Carlo generation, $\epsilon^{\rm nom}_{\rm MC}$

The uncertainty on $\epsilon^{\rm eff}_{\rm MC}$ due to MC statistics is negligible as $70,000$ events were used, much more than any of the data sub-sample sizes.

Muon identification efficiency, $\epsilon_{\mu\rm ID}$, Muon tracking efficiency, $\epsilon_{\mu\rm trk}$, Trigger efficiency, $\epsilon_{\rm trig}$ Because these efficiencies are measured on each separate data sample, the statistical uncertainties associated with this measurement are among the largest uncertainties in this analysis. Even in the largest subsample considered these statistical uncertainties are several times larger than the systematics associated with muon ID and muon tracking efficiency as determined in the p17 muon ID certification note [3]. We therefore neglect any systematic effects other than the statistical uncertainty of these efficiencies. Systematic effects associated with trigger efficiency measurements are covered by the comparison of yields obtained with different triggers in the same data sample, described in Section 8.1.

Luminosity profile reweighting, $\epsilon_{\rm lumi}$, Beam shape reweighting, $\epsilon_{\rm beam}$ The shape of the luminous region at DØ depends on shapes of the p and $\overline{p}$ bunches and on the β^*_x and β^*_y of the interaction point. These parameters were determined and used to reweight Monte Carlo events, which were generated with a gaussian of width 25 cm. The determination of β^* is described in DØ Note 4735[4] and the fits to the beam shape are described in more detail in DØ note 5142[11] (from which, with modifications, thi section has been excerpted). The method used is similar to that used by CDF (CDF Note, 7935) but the DØ analysis explicitly includes the observed dependence on run epoch and instantaneous luminosity where CDF integrates over the full data sample.

The z dependence of the luminosity can be described by:

$$\frac{d\mathcal{L}(z)}{dz} = N_p N_{\bar{p}} \frac{1}{\sqrt{2\pi}\sigma_z} \frac{\exp^{-(z-z_{0z})^2/2/\sigma_z^2}}{4\pi\sigma_x(z)\sigma_y(z)} \tag{6}$$

Here z_{0z} and σ_z describe the overlap of the gaussian proton and anti-proton beam bunches, which is also a gaussian, with a possible offset relative to the nominal interaction point (IP). $\sigma_x(z)$ and $\sigma_y(z)$ represent the transverse size of the beam spot and vary as a function of z as follows.

$$\sigma_T^2(z) = \frac{1}{6\pi\gamma}\epsilon_T\beta_T^*(1+\frac{(z-z_{0T})^2}{\beta_T^{*2}}) \quad (7)$$

Here T is either x or y, γ is the γ of the beam particles, ϵ_T is the emittance , β_T^* is the beta parameter and z_{0T} is the minimum of the β function in direction T.

The observed vertex distributions for zero bias events were fit using these functional forms, with the x, y parameters determined in Note 4735 and with σ_z and z_0 as free parameters. Due to improvements in the machine parameters β^* was reduced from 55 cm at the beginning of the run to 30 cm at the end of Run IIa. σ_z remained close to the 40 cm measured by CDF early in the run but was found to vary by up to 5 cm as the instantaneous luminosity changed and as RunIIa progressed. These variations causes variations of 3-5% in the fraction of beam interactions falling within a 40 cm cut and thus could have significant effects on cross section measurements if not accounted for correctly.

The fits were checked by changing the fit ranges from 40 to 60 cm and by increasing the input β^* values by 2.5 cm. The integrals of $\frac{d\mathcal{L}z}{dz}$ were then compared as a function of the integral bounds. The analytically calculated acceptance changed for a 40 cm cut by a maximum of 1.5 % and 0.4-0.6% for a 60 cm cut. These fits are implemented in wzcross_sample/src/BeamWeight.cpp.

All Monte Carlo events are overlaid by actual zero bias events recorded during DØ physics data taking. This introduces proper luminosity dependence of noise levels into the simulation and thus makes reconstruction efficiencies luminosity depend. For each trigger in each subsample of RunIIa, the MC sample and the MC tag and probe muon ID and tracking efficienies are reweighted to match the instantaneous luminosity distribution obtained from the DØ luminosity counters for the respective dataset and trigger. The beam shape is then reweighted as a function of the instantaneous luminosity of the zero bias overlay event and the z position of the true Z boson production vertex in MC.

Next-to-leading order reweighting, $\epsilon_{\mathbf{NLO}}$ This quasi-leading-order PYTHIA model used for $\epsilon_{\mathrm{MC}}^{\mathrm{nom}}$ receives next-to-leading order (NLO) corrections through event cross section reweighting as a function of Z boson p_t and rapidity using the RESBOS[15] package and the NLO CTEQ6.1M PDF set. RESBOS has been found to well-describe transverse momentum and rapidity distributions for inclusive Z^0 production in the electron channel[16].

The NLO corrections tend to be small. This likely reflects the fact that the major NLO effect on the Z^0 production rate is an increase by an overall $K-$factor, which is irrelevant for the efficiency (but not for the absolute luminosity!). NLO/LO differences in the Z^0 rapidity and p_T distributions are fairly modest. These also get washed out by the finite length of the interaction region and by resolution effects.

PDF reweighting The effect on $\epsilon_{\mathrm{MC}}^{\mathrm{eff}}$ of varying the choice of PDF was investigated using CTEQ6.1M error sets. The CTEQ6.1M PDF set has a series of free parameters which have been set to optimize the agreement between the global PDF fit and data [12]. CTEQ6.1 has, in addition to the central sample, 20 pairs of PDFs displaced 'up' (S_+) and 'down' (S_-) one sigma along each of these free parameters with respect to the nominal parameter set (S_0).

The uncertainty ($\Delta X_{\pm}$) on an observable (X), such as $\epsilon_{\rm MC}^{\rm eff}$, is the quadrature sum of the uncertainties on each parameter.

$$\Delta X_{\pm} = \left(\sum_{i=1}^{N_p} \left[X(S_{\pm}^i) - X(S_0^i) \right]^2 \right)^{1/2} \tag{8}$$

The PDF uncertainty in this analysis is evaluated in two largely independent ways. One method is using events generated with RESBOS+CTE6.1M and all 40 error PDFs to create 41 different sets of Z p_t and rapidity reweighting distributions which are used to correct Pythia events. This procedure should take PDF uncertainties from higher order processed into account that are not simulated in Pythia.

The second method is to reweight Pythia from CTEQ6L1 to CTEQ6.1M and error PDFs using Pythia PDF input arguments x and Q^2. Although this method neglects uncertainty contributions from particles in loops, this effect seems to be negligible, as the uncertainties derived from both methods agree to within better than a few percent relative.

The uncertainty in $\epsilon_{\rm MC}^{\rm eff}$ due to the choice of PDF is found to be around 1% using this method. The uncertainty is evaluated separately for each trigger and dataset because it depends slightly on the acceptance region of the trigger that was used.

7.1.2 Calorimeter data quality, $\epsilon_{\rm DQ}$

Events affected by calorimeter noise are removed in order to avoid a bias of the isolation cut efficiency measurement. $\epsilon_{\rm DQ}$ is measured on the fraction of the CSG 2MUhighpt skim associated with the corresponding data sample. This measurement is unbiased because no calorimeter readout is used in the event selection for this skim.

7.1.3 Timing cuts, $\epsilon_{\rm time}$

see above

7.1.4 Level 1 fast Z cut, $\epsilon_{{\rm fast}Z}$

see above

7.1.5 Level 3 track matching, $\epsilon_{L3{\rm match}}$

see above

7.1.6 Trigger pre-scale, $\epsilon_{\rm pre}$

see above

7.2 Data vs. Simulation Comparisons

This analysis entails the generation of thousands of different plots covering the 14 statistically significant trigger epochs and the several trigger cross check samples per epoch. A small

sample of these follow. Distributions of selected kinematic quantites are shown for each trigger epoch. While the plots are necessarily small, it is hoped that the general quality of data vs. Monte Carlo simulations can be discerned. Kolmogorov Smirnov probabilities are given on top of each plot. All data plots are overlaid with Monte Carlo simulated events with a γ/Z invariant mass range of 15-1000 GeV/c^2 for both $\mu\mu$ and $\tau\tau$ (shaded) final states. The MC contribution is normalized to data in each plot separately.

7.3 Comparisons between the epochs

Figures 5–9 show the leading muon p_T, the trailing muon p_T, the inclusive muon ϕ, the inclusive muon detector η, and the inclusive muon physics η, respectively. A Kolmogorov-Smirnov (KS) test statistic is computed for each distribution in each epoch. We find the KS probability to be satisfactory for all cases. The agreement between data and Monte Carlo for the detector η distributions provides evidence that η dependent efficiency effects are properly being taken into account and that any residual next-to-leading order cross section effects that could manifest themselves at large $|\eta|$ are small.

The next three figures provide examples of distributions that fail to agree in detail, but which nevertheless good enough in that all cuts are placed well beyond the extent of the observed distributions. Figure 10 is the distance-of-closest-approach DCA in the xy plane for muons that have at least two SMT hits. Figure 11 is the distance-of-closest-approach DCA for muons that lack at least two SMT hits. Figure 12 is the difference in z positions Δz at their distance of closest approach.

The final four plots show the dimuon invariant mass over the range $0 - 300$ GeV/c^2, Fig. 13, the dimuon p_T distribution, Fig. 14, the dimuon ϕ distribution, Fig. 15, and the dimuon z vertex distribution z_0, Fig. 16. The good agreement between data and Monte Carlo for the first shows that muon resolution effects are being properly modelled and that no large systematic errors are being introduced by the rather agressive cut (chosen to match the electron channel analysis) around the Z mass. The broad distribution of $M_{\mu\mu}$ under the Z peak is consistent with continuum Drell-Yan production. No evidence exists for any strongly mass or p_t dependent mis-reconstruction effects. The Z transverse momentum likewise shows that resolution is being properly taken into account, and that the RESBOS weighting is correctly implemented. One can see that the z vertex distribution is well-modelled in the central region for $|z_0| < 40$ cm.

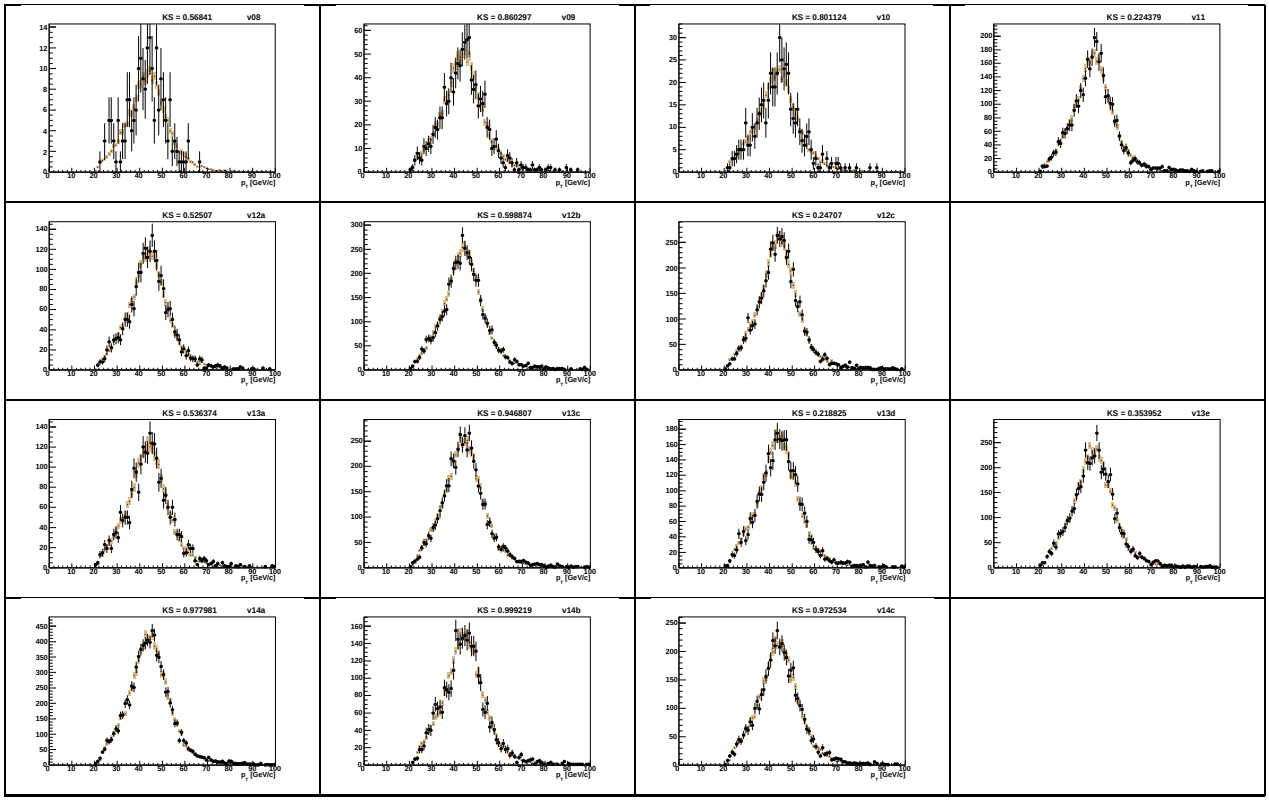

Figure 5: A comparison of the p_T of the leading muon between the 14 different trigger epochs. On each plot the horizontal scale is the p_T of the muon in GeV; full scale is 100 GeV. The vertical scale is the number of events. The data are the points with error bars. The shaded histogram represents the Monte Carlo prediction. The Kolmogorov-Smirnov test statistic between data and simulation is written at the top of each plot. The first row contains, from left to right, the trigger epochs v08, v09, v10, and v11. The second contains, from left to right, the trigger epochs v12a, v12b, and v12c. The third row contains, from left to right, the trigger epochs v13a, v13c, v13d, and v13e. The fourth row contains, from left to right, the trigger epochs v14a, v14b, v14c.

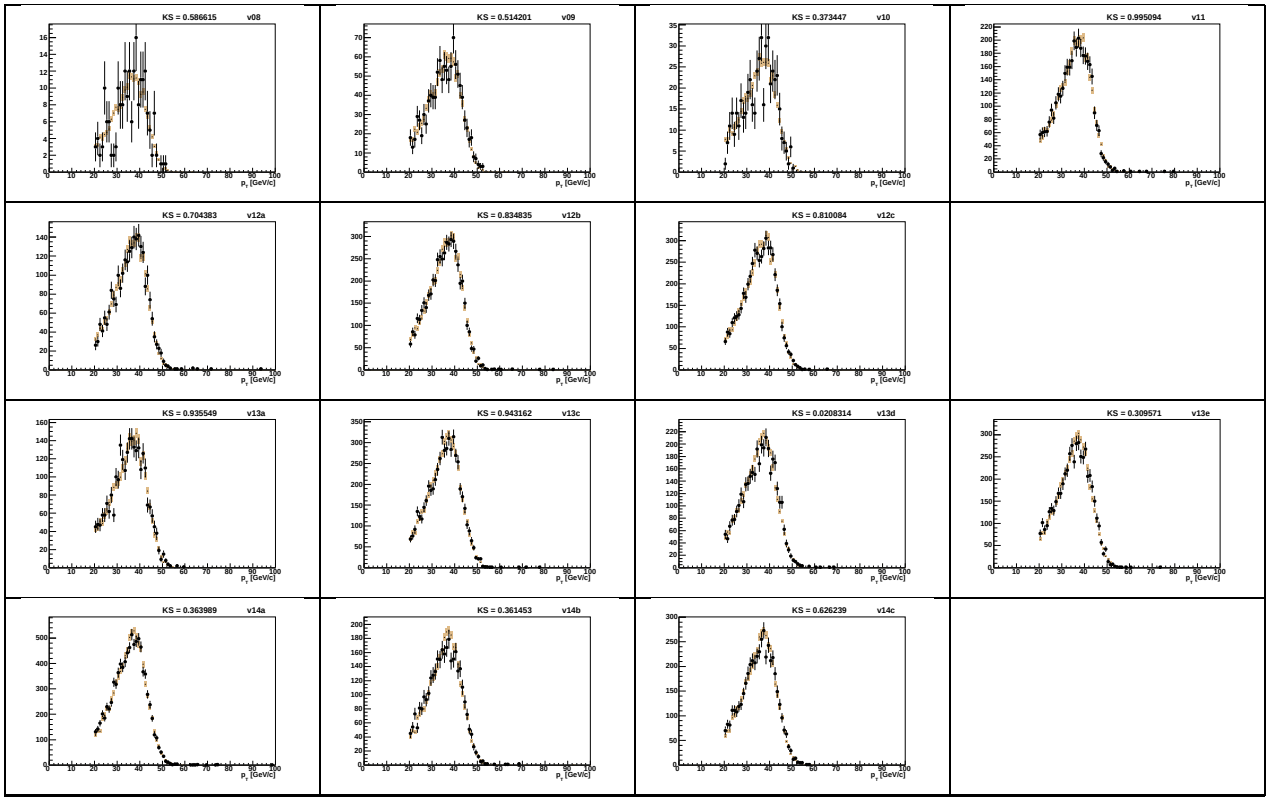

Figure 6: A comparison of the p_T of the trailing muon between the 14 different trigger epochs. On each plot the horizontal scale is the p_T of the muon in GeV; full scale is 100 GeV. The vertical scale is the number of events. The data are the points with error bars. The shaded histogram represents the Monte Carlo prediction. The Kolmogorov-Smirnov test statistic between data and simulation is written at the top of each plot. The first row contains, from left to right, the trigger epochs v08, v09, v10, and v11. The second contains, from left to right, the trigger epochs v12a, v12b, and v12c. The third row contains, from left to right, the trigger epochs v13a, v13c, v13d, and v13e. The fourth row contains, from left to right, the trigger epochs v14a, v14b, v14c.

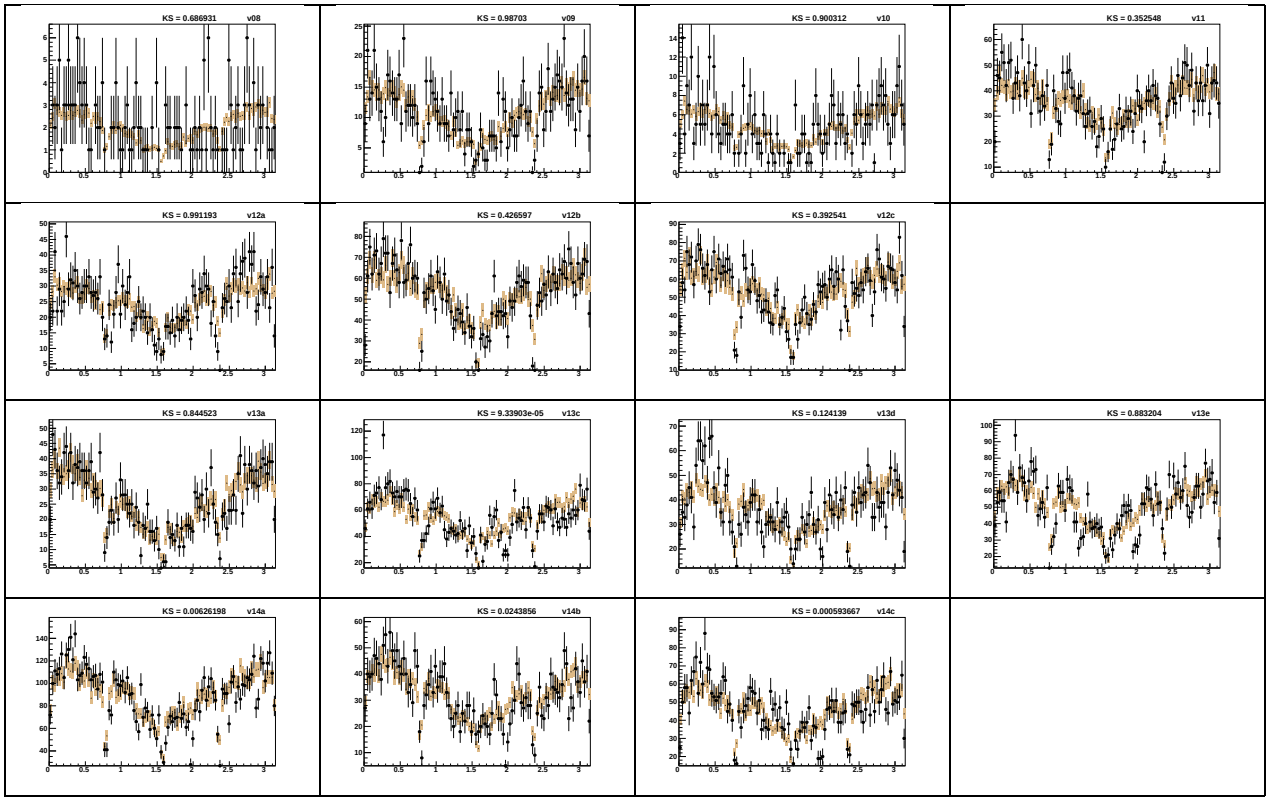

Figure 7: A comparison of the ϕ of the muons in Z candidates between the 14 different trigger epochs. The vertical scale is the number of events. The data are the points with error bars. The shaded histogram represents the Monte Carlo prediction. The Kolmogorov-Smirnov test statistic between data and simulation is written at the top of each plot. The first row contains, from left to right, the trigger epochs v08, v09, v10, and v11. The second contains, from left to right, the trigger epochs v12a, v12b, and v12c. The third row contains, from left to right, the trigger epochs v13a, v13c, v13d, and v13e. The fourth row contains, from left to right, the trigger epochs v14a, v14b, v14c.

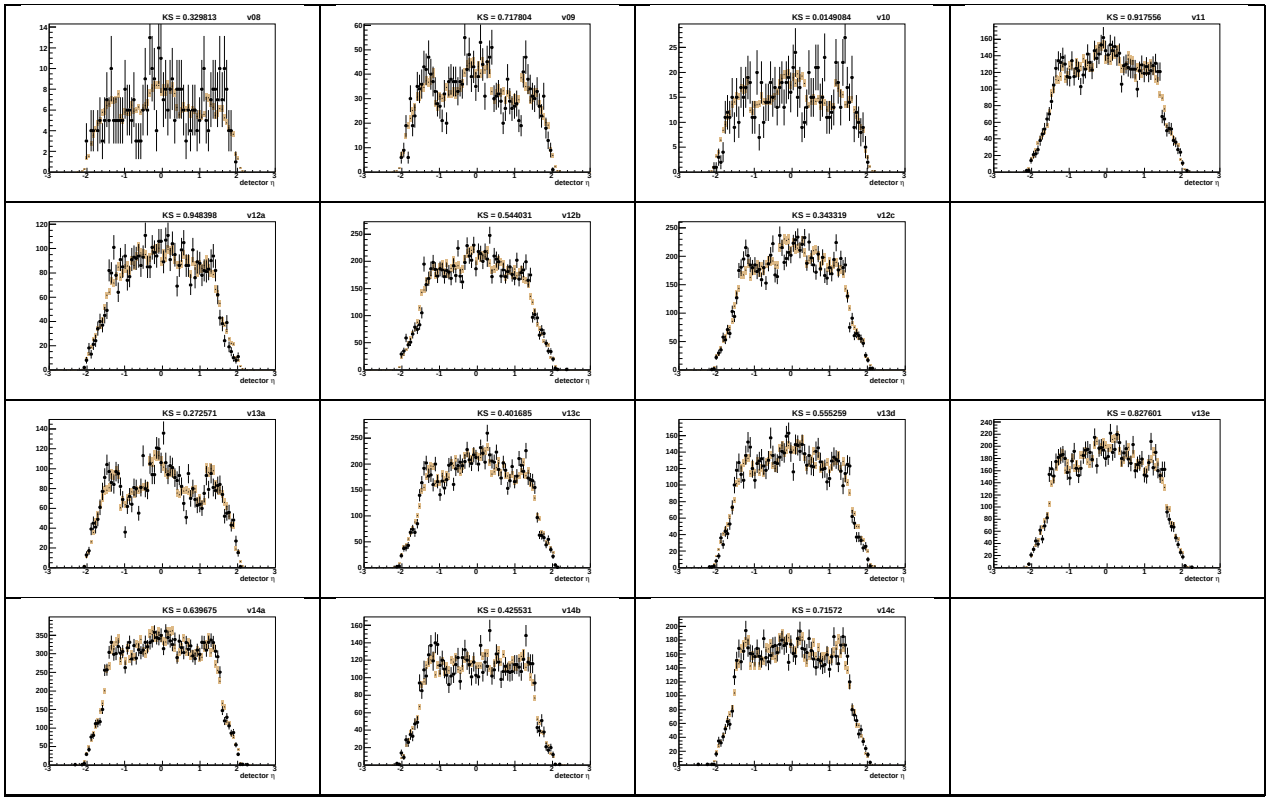

Figure 8: A comparison of the muon detector pseudorapidity between the 14 different trigger epochs. On each plot the horizontal scale is muon η; full scale is -3 to 3. The vertical scale is the number of events. The data are the points with error bars. The shaded histogram represents the Monte Carlo prediction. The Kolmogorov-Smirnov test statistic between data and simulation is written at the top of each plot. The first row contains, from left to right, the trigger epochs v08, v09, v10, and v11. The second contains, from left to right, the trigger epochs v12a, v12b, and v12c. The third row contains, from left to right, the trigger epochs v13a, v13c, v13d, and v13e. The fourth row contains, from left to right, the trigger epochs v14a, v14b, v14c.

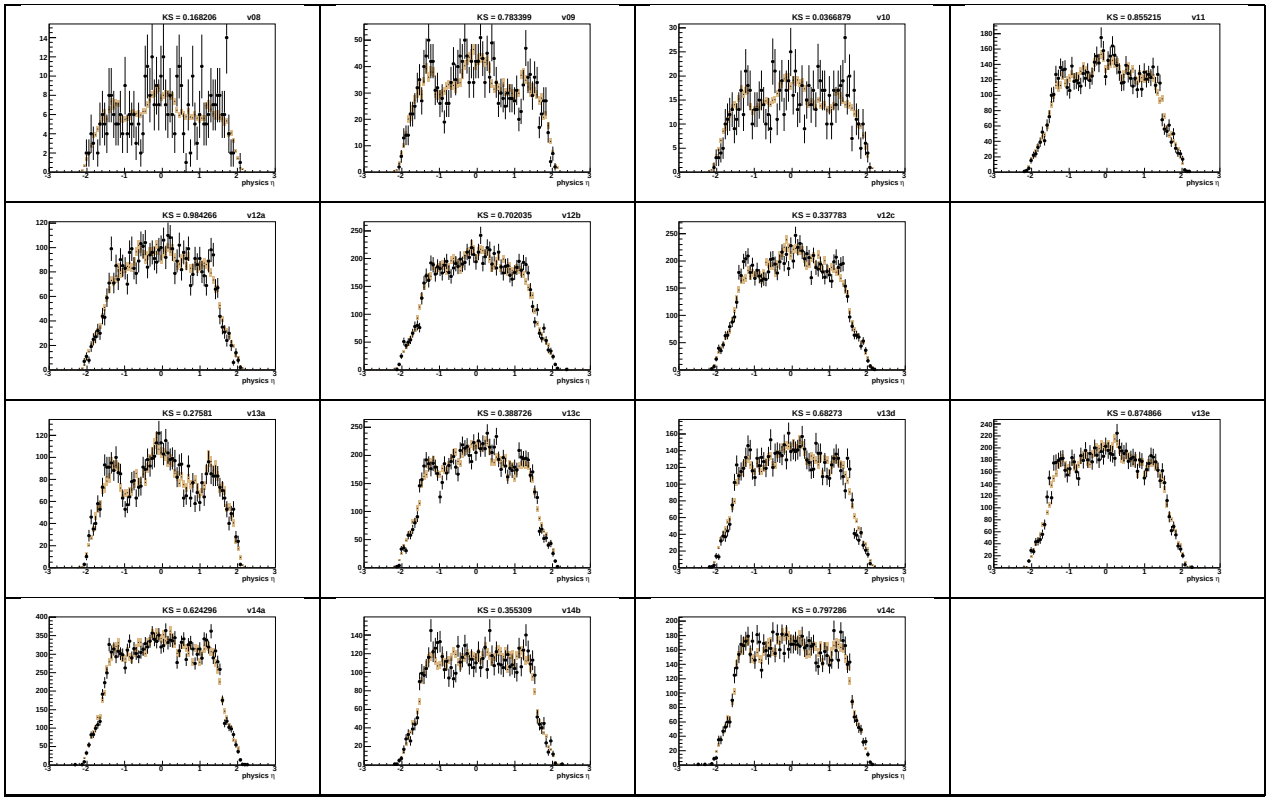

Figure 9: A comparison of the muon physics pseudorapidity between the 14 different trigger epochs. On each plot the horizontal scale is muon η; full scale is -3 to 3. The vertical scale is the number of events. The data are the points with error bars. The shaded histogram represents the Monte Carlo prediction. The Kolmogorov-Smirnov test statistic between data and simulation is written at the top of each plot. The first row contains, from left to right, the trigger epochs v08, v09, v10, and v11. The second contains, from left to right, the trigger epochs v12a, v12b, and v12c. The third row contains, from left to right, the trigger epochs v13a, v13c, v13d, and v13e. The fourth row contains, from left to right, the trigger epochs v14a, v14b, v14c.

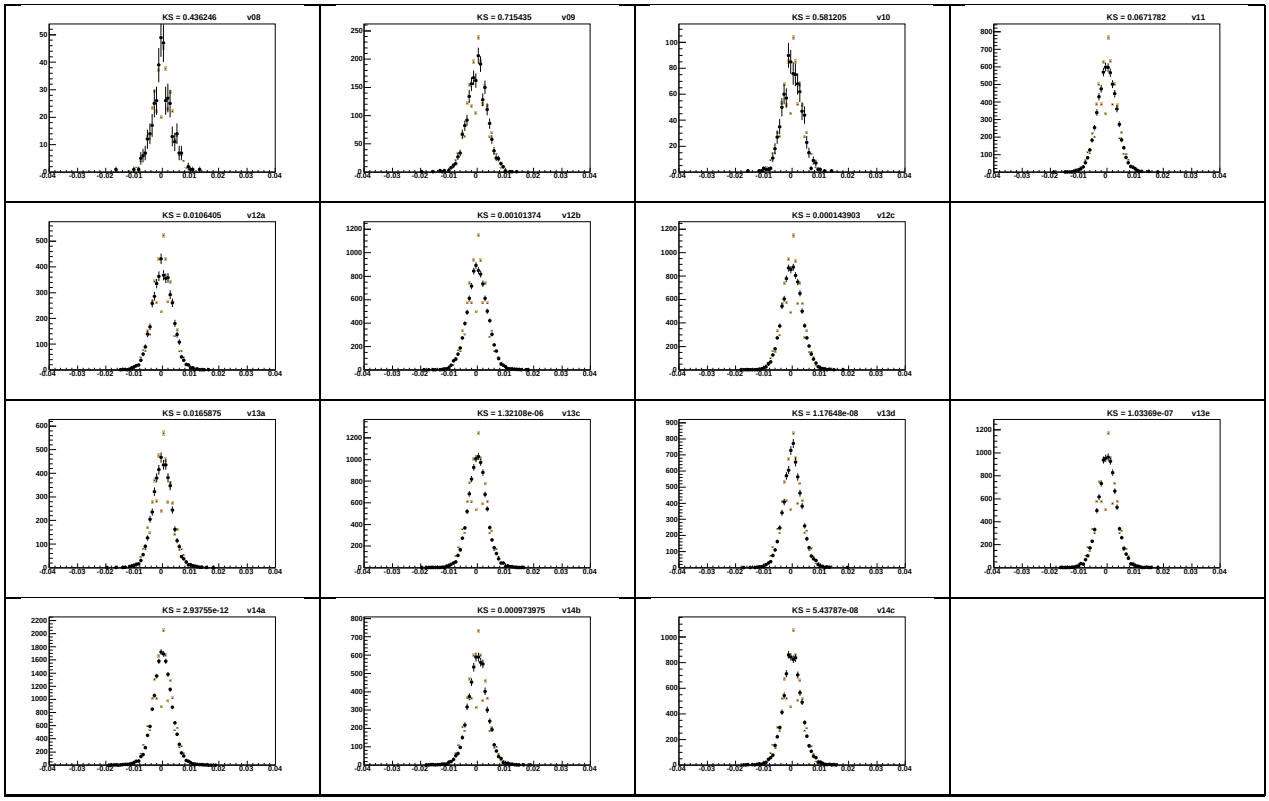

Figure 10: A comparison of the muon distance of closest approach DCA_{SMT} for muons with at least two SMT hits between the 14 different trigger epochs. On each plot the horizontal scale is muon DCA_{SMT}; full scale is -0.2 to 0.2 cm. The vertical scale is the number of events. The data are the points with error bars. The shaded histogram represents the Monte Carlo prediction. The Kolmogorov-Smirnov test statistic between data and simulation is written at the top of each plot. The first row contains, from left to right, the trigger epochs v08, v09, v10, and v11. The second contains, from left to right, the trigger epochs v12a, v12b, and v12c. The third row contains, from left to right, the trigger epochs v13a, v13c, v13d, and v13e. The fourth row contains, from left to right, the trigger epochs v14a, v14b, v14c.

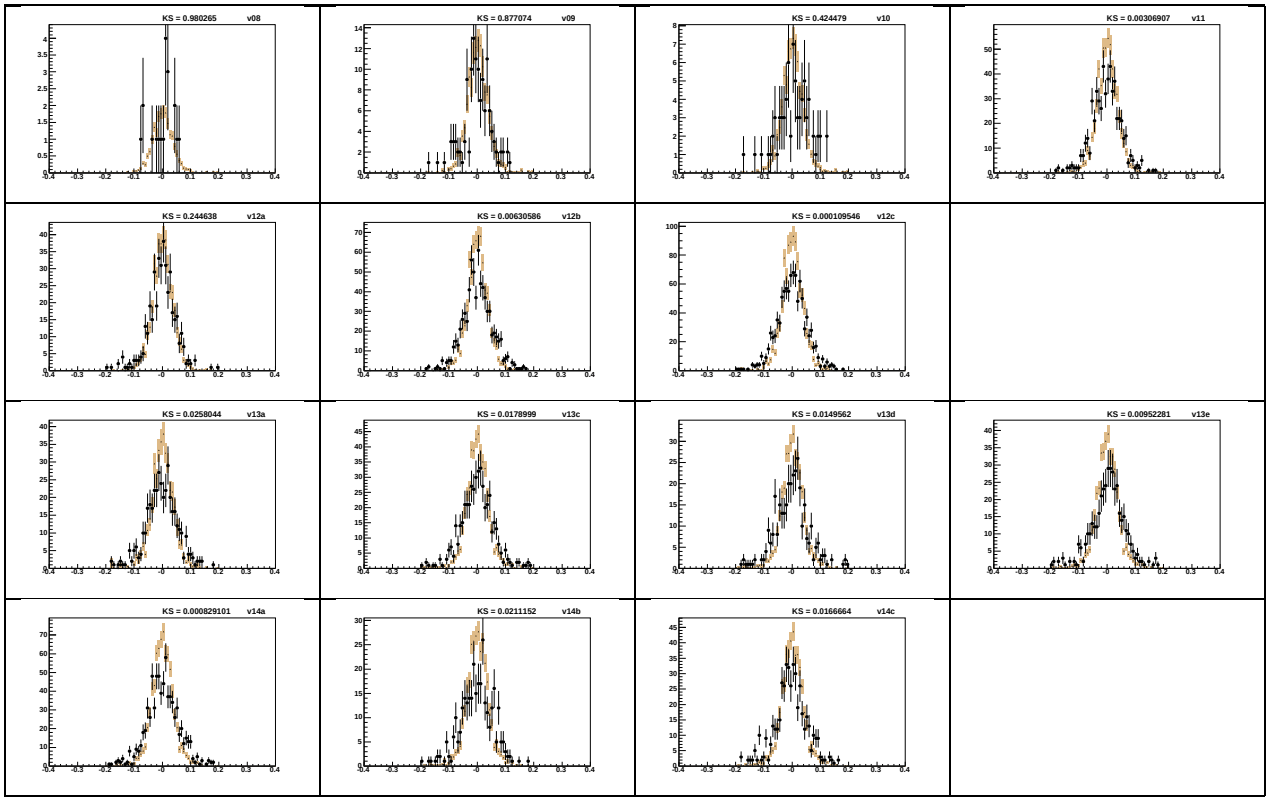

Figure 11: A comparison of the muon distance of closest approach DCA_{CFT} for muons without at least two SMT hits between the 14 different trigger epochs. On each plot the horizontal scale is muon DCA_{CFT}; full scale is -2 to 2 cm. The vertical scale is the number of events. The data are the points with error bars. The shaded histogram represents the Monte Carlo prediction. The Kolmogorov-Smirnov test statistic between data and simulation is written at the top of each plot. The first row contains, from left to right, the trigger epochs v08, v09, v10, and v11. The second contains, from left to right, the trigger epochs v12a, v12b, and v12c. The third row contains, from left to right, the trigger epochs v13a, v13c, v13d, and v13e. The fourth row contains, from left to right, the trigger epochs v14a, v14b, v14c.

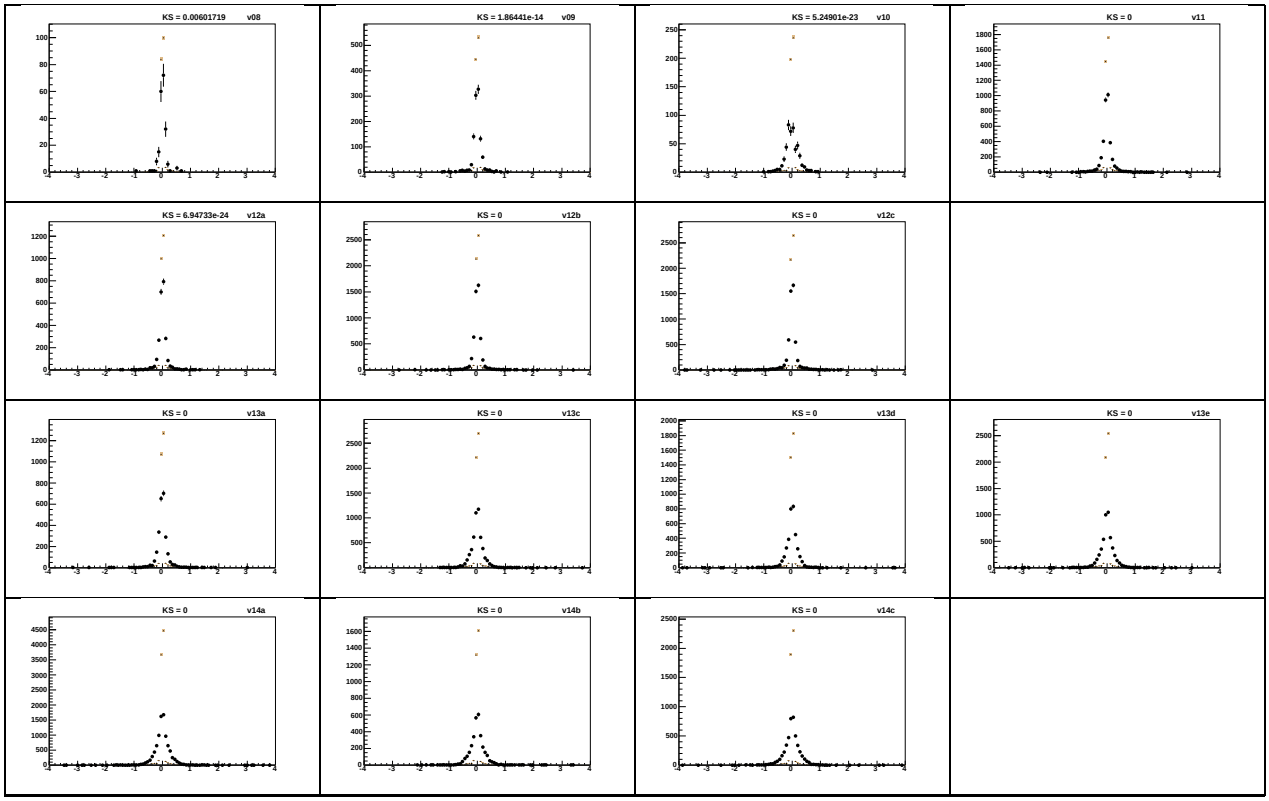

Figure 12: A comparison of the difference is reconstructed muon z, Δz between the 14 different trigger epochs. On each plot the horizontal scale is muon Δz; full scale is -10 to 10 cm. The vertical scale is the number of events. The data are the points with error bars. The shaded histogram represents the Monte Carlo prediction. The Kolmogorov-Smirnov test statistic between data and simulation is written at the top of each plot. The first row contains, from left to right, the trigger epochs v08, v09, v10, and v11. The second contains, from left to right, the trigger epochs v12a, v12b, and v12c. The third row contains, from left to right, the trigger epochs v13a, v13c, v13d, and v13e. The fourth row contains, from left to right, the trigger epochs v14a, v14b, v14c.

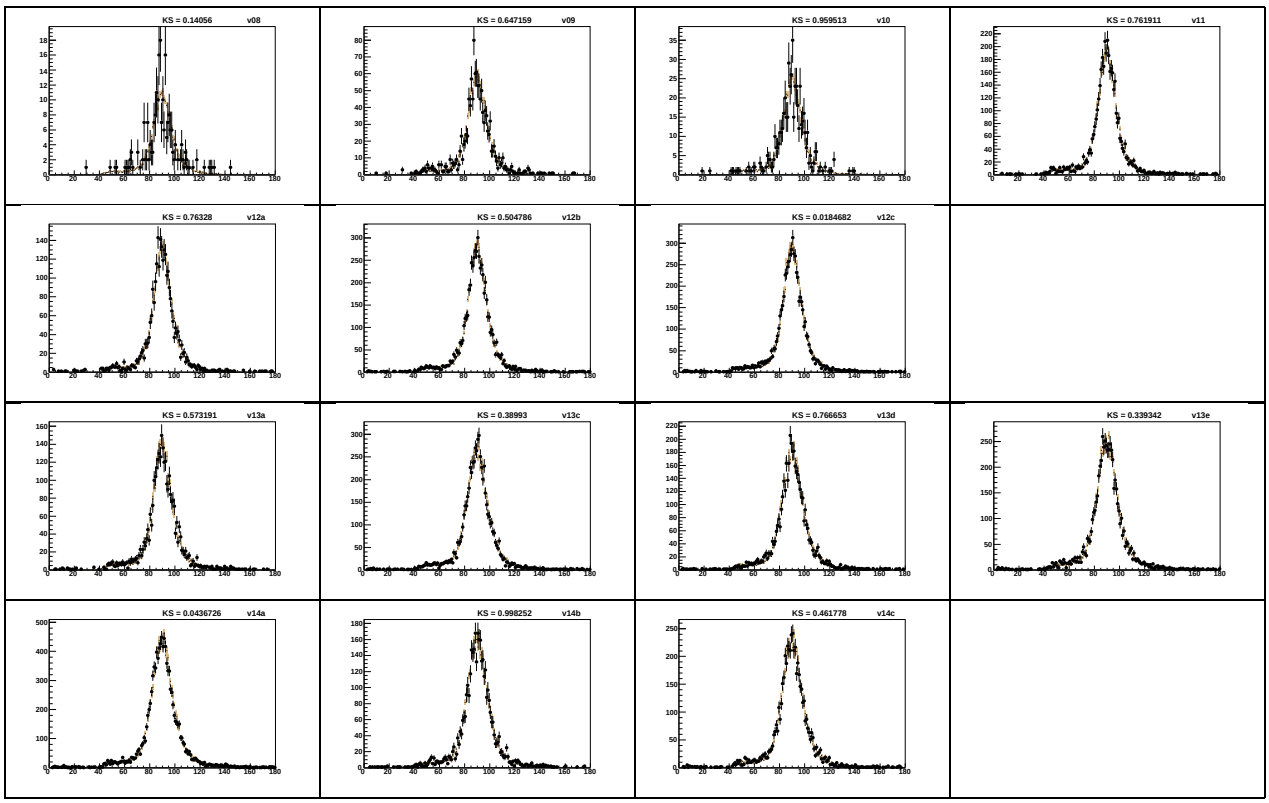

Figure 13: A comparison of the dimuon mass distribution between the 14 different trigger epochs. On each plot the horizontal scale is the dimuon mass in GeV/c^2; full scale is 0-300 GeV/c^2. Selected events lie within the mass range 70-110 GeV/c^2. The vertical scale is the number of events. The data are the points with error bars. The shaded histogram represents the Monte Carlo prediction. The filled histogram peaking below the Z mass shows the $Z \to \tau\tau$ background contribution. The Kolmogorov-Smirnov test statistic between data and simulation is written at the top of each plot. The first row contains, from left to right, the trigger epochs v08, v09, v10, and v11. The second contains, from left to right, the trigger epochs v12a, v12b, and v12c. The third row contains, from left to right, the trigger epochs v13a, v13c, v13d, and v13e. The fourth row contains, from left to right, the trigger epochs v14a, v14b, v14c.

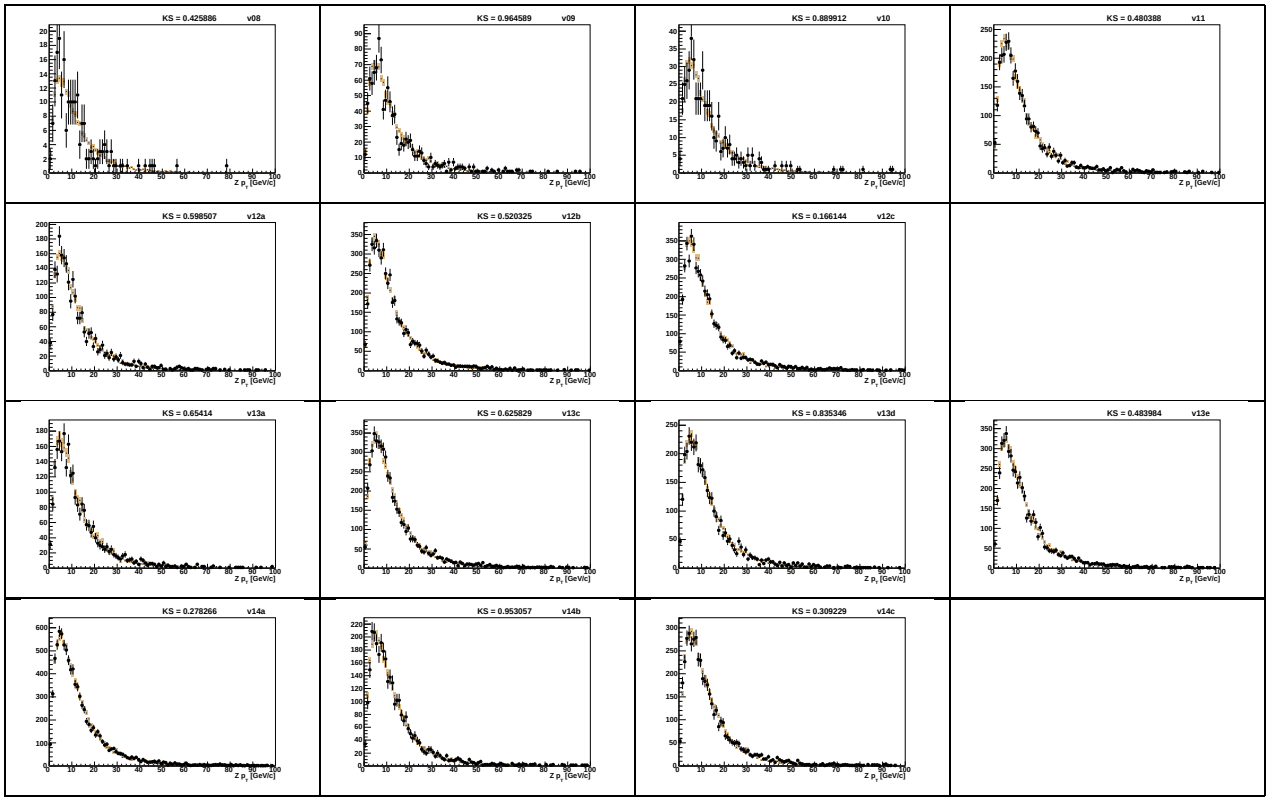

Figure 14: A comparison of the dimuon p_T distribution between the 14 different trigger epochs. On each plot the horizontal scale is the dimuon $p_T$in GeV/c; full scale is 0-200 GeV/c. Selected events lie within the mass range 70-110 GeV/c^2. The vertical scale is the number of events. The data are the points with error bars. The shaded histogram represents the Monte Carlo prediction. The Kolmogorov-Smirnov test statistic between data and simulation is written at the top of each plot. The first row contains, from left to right, the trigger epochs v08, v09, v10, and v11. The second contains, from left to right, the trigger epochs v12a, v12b, and v12c. The third row contains, from left to right, the trigger epochs v13a, v13c, v13d, and v13e. The fourth row contains, from left to right, the trigger epochs v14a, v14b, v14c.

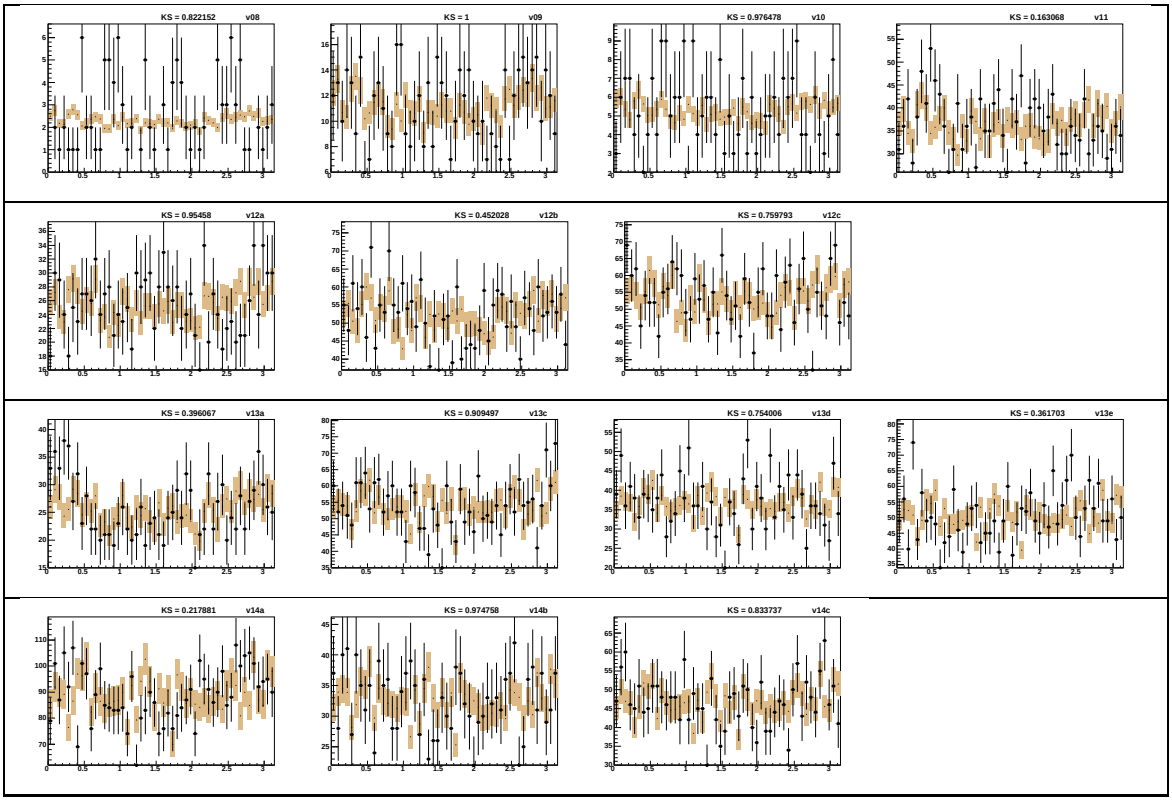

Figure 15: A comparison of the dimuon phi distribution between the 14 different trigger epochs. On each plot the horizontal scale is the dimuon ϕ in rad full scale is 2π. Selected events lie within the mass range 70-110 GeV/c^2. The vertical scale is the number of events. The data are the points with error bars. The shaded histogram represents the Monte Carlo prediction. The Kolmogorov-Smirnov test statistic between data and simulation is written at the top of each plot. The first row contains, from left to right, the trigger epochs v08, v09, v10, and v11. The second contains, from left to right, the trigger epochs v12a, v12b, and v12c. The third row contains, from left to right, the trigger epochs v13a, v13c, v13d, and v13e. The fourth row contains, from left to right, the trigger epochs v14a, v14b, v14c.

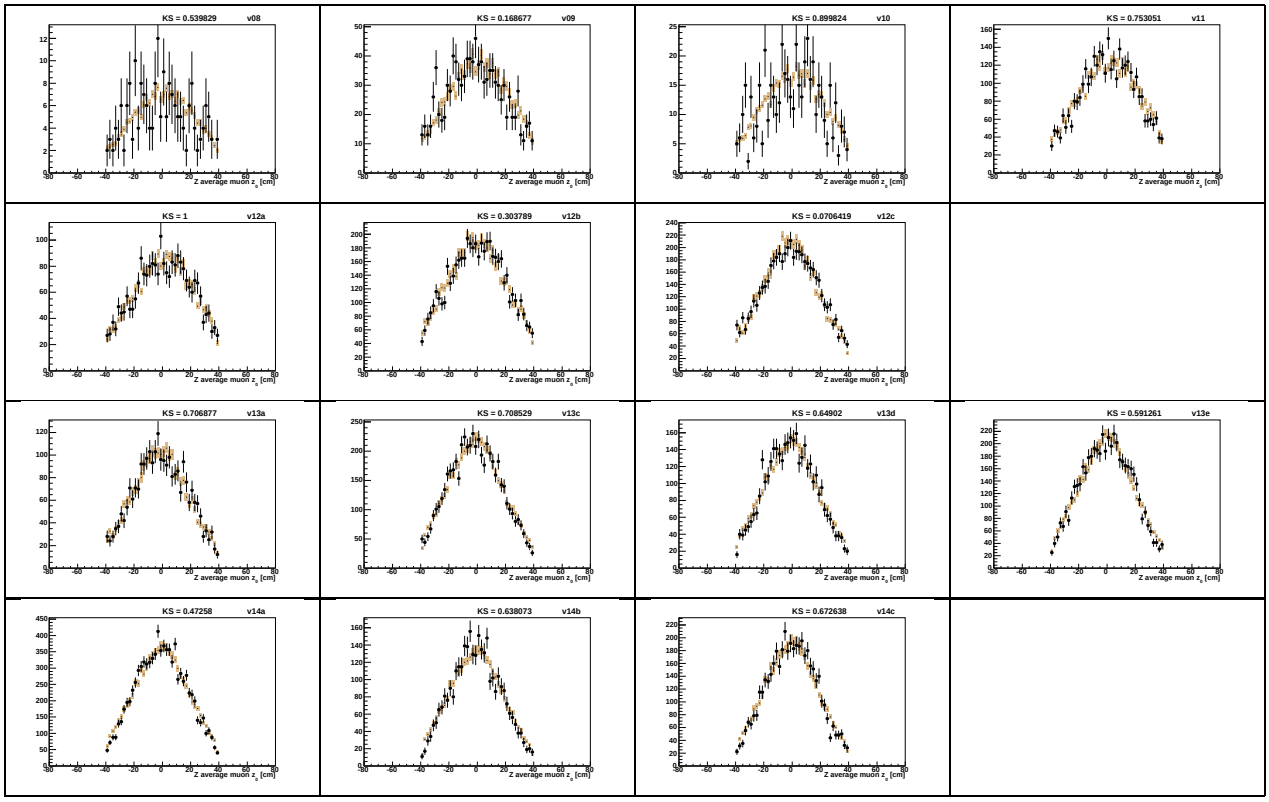

Figure 16: A comparison of the dimuon z vertex distribution between the 14 different trigger epochs. On each plot the horizontal scale is the dimuon z vertex in cm; full scale is -80 to 80 cm. Selected events lie within the mass range 70-110 GeV/c^2. The vertical scale is the number of events. The data are the points with error bars. The shaded histogram represents the Monte Carlo prediction. The Kolmogorov-Smirnov test statistic between data and simulation is written at the top of each plot. The first row contains, from left to right, the trigger epochs v08, v09, v10, and v11. The second contains, from left to right, the trigger epochs v12a, v12b, and v12c. The third row contains, from left to right, the trigger epochs v13a, v13c, v13d, and v13e. The fourth row contains, from left to right, the trigger epochs v14a, v14b, v14c.

8 Systematic studies

This section contains studies of potential systematic effects of particular relevance for this analysis.

8.1 Trigger efficiency systematics

Most parts of this analysis are controlled to the level of one percent uncertainty or better. Backgrounds are almost negligible, all relevant distributions are modeled extremely well or only cut on very loosely. The statistical uncertainties on the number of selected events and on the efficiency measurements are among the largest uncertainties in the analysis. However, these uncertainties would become much less significant in a combination of the different periods. Beam shape uncertainty and PDF unertainty each contribute at the level of a percent or more. Muon ID and track reconstruction efficiencies have been studied in detail by the muon ID group and no significant systematics were found other than beam shape and luminosity dependence, which we both correct for to the best of our knowledge. Furthermore, we apply these efficiencies as mere corrections to a very detailed and sophisticated Monte Carlo simulation, further reducing the likelihood of systematic problems.

The single large remaining uncertainty at this stage is the trigger efficiency measurement. By repeating the Z yield measurement with different triggers and comparing the yields we obtain an estimate of the trigger efficiency precision even without knowledge about reasons for biases. This method checks not only the efficiency determination itself, but also the event weight calculation. This is an extremely powerful cross check that has already led to the discovery of major problems, for example

- wrong translation of trigger names to individual trigger terms
- wrong cuts in efficiency measurements, e.g. number of hits on L3 tracks
- data quality problems, e.g. missing L1CTT track parameter readout

Assuming that the actual efficiency measurement and its imminent uncertainties are fully understood and under control, the Z yields obtained using different triggers on the same data sample should be the same within the statistical and systematic uncertainties. Any latent and hidden systematic complication should manifest itself in such a test.

For each trigger epoch we chose in addition to the reference trigger a set of test triggers (see Table 4). The Z yields were calculated as described in Section 7 except that for this test yields were obtained for the biggest subset of all runs in which all triggers from one set were used and not pre-scaled. In sample v09 we allow runs where one trigger is prescaled because mu2ptxatxx_fz is never unprescaled in that sample.

The yield from each test trigger was then compared to the yield of the reference trigger of that particular trigger epoch. Simple Gaussian error propagation was used to calculate the total error on the difference between test and reference yield taking into account correlations arising from trigger and ID efficiencies. In the same way events in those sub-samples fired by both the reference and the test trigger accounted for correlated statistical error.

The results of this test are summarized in Figure 17. Each plot represents one trigger epoch. Shown are for each trigger epoch the test and reference trigger yields. The error bars

correspond to the total error on the difference between a test trigger and the reference trigger yield as described above. The test reveals an overall good agreement between reference and test triggers. However, systematic patterns as in the v12 trigger epochs or the outliers in the v13 trigger epochs will lead to an increased total systematic error on the final Z yields for each trigger epoch.

In each period we assign the maximum range of yield differences with respect to the central value trigger as a systematic uncertainty. Z yields from samples with identical trigger choice (v08–v09, v11-v12c, v13c-v13e, v14a-v14c) are added, and the relative variation of the yield sum is assigned as systematic uncertainty to all contributing samples. This reduces the effect of double counting the statistical uncertainties of both data selection and trigger efficiencies. The individual results are given in the following section. In many data periods the trigger variation uncertainty is highly asymmetric, because the central value trigger was not chosen according to some mean yield. The choice of central value triggers was determined by total number of selected events (thus maximal integrated luminosity), and preference was given to single muon triggers in preparation for a future $W \to \mu\nu$ analysis.

8.2 Instantaneous luminosity dependence

The yield measurement was checked for any potential instantaneous luminosity dependence. This is important for two reasons:

- Some efficiency components, e.g. the track reconstruction efficiency, are known to be luminosity dependent. Great care has been taken to reproduce luminosity dependent effects in Monte Carlo simulation by zero bias event overlay with properly reweighted luminosity profiles, but it is a priori not guaranteed that this approach addresses the issue fully.

- For the purpose of cross-checking the DØ luminosity measurment, it is desirable to check for any biases varying with instantaneous luminosity.

This cross check was restricted to v13 and v14 data samples because of their larger range of luminosities, larger datasets, and because all types of efficiencies that were used in v8-v12 are also used in v13-v14, i.e. we do not expect to gain any additional information by looking at older data samples.

The v13 and v14 samples were split into three bins in instantaneous luminosity of roughly equal size in terms of integrated luminosity. The corresponding numbers were made available in Ref. [17]. The absolute scale of the luminosity is not available from these numbers, thus the analysis remains blinded in that respect.

All efficiency measurements were redone separately for the three luminosity bins per data epoch. Monte Carlo luminosity profiles were corrected accordingly. To maintain a reasonable sample size in each luminosity bin, the acceptance, efficiency and background corrected Z yield measured in each data epoch was added to v13 respectively v14 totals in each of the three luminosity bins. The yield sums were then divided by their normalized integrated luminosity fraction as obtained from Ref. [17].

Figures 18 and 19 show the result of this study. Both v13 and v14 distributions are compatible with being flat.

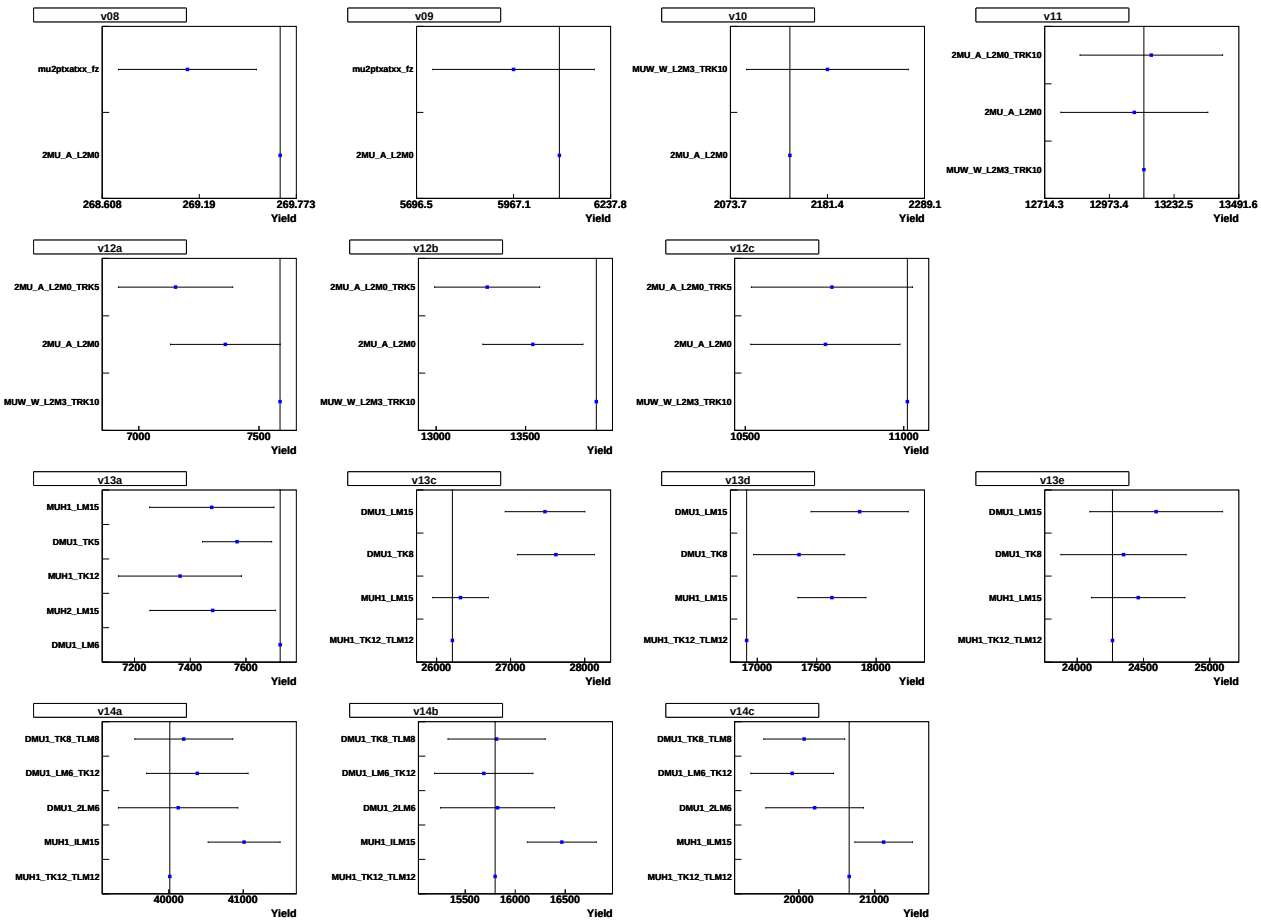

Figure 17: A comparison of the Z yields between different triggers for the 14 different trigger epochs. Each plot shows the Z event yield obtained with the reference trigger (vertical line) and the yields obtained with a selection of additional triggers available during that trigger epoch. The yields are normalized to the largest common data sample in which all of the triggers in that trigger epoch were used without pre-scales. The error bars represent the error on the yield difference to the central value trigger yield. The error calculation takes into account all correlations between the triggers within one trigger epoch.
The first row contains, from left to right, the trigger epochs v08, v09, v10, and v11. The second contains, from left to right, the trigger epochs v12a, v12b, and v12c. The third row contains, from left to right, the trigger epochs v13a, v13c, v13d, and v13e. The fourth row contains, from left to right, the trigger epochs v14a, v14b, v14c.

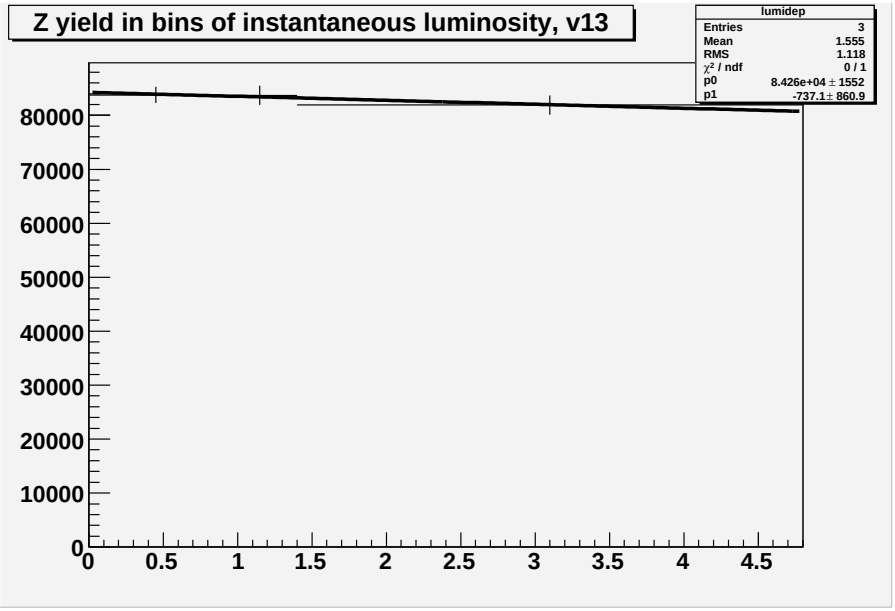

Figure 18: Sum of Z yields in three instantaneous luminosity bins derived from data epochs v13a–e, divided by a normalized integrated luminosity fraction. The error bars indicate the statistical uncertainties of selection and efficiency determination. The distribution is compatible with being flat, as indicated by the slope of the superimposed linear fit. A constant value fit results in a χ^2/dof of 0.8/2.

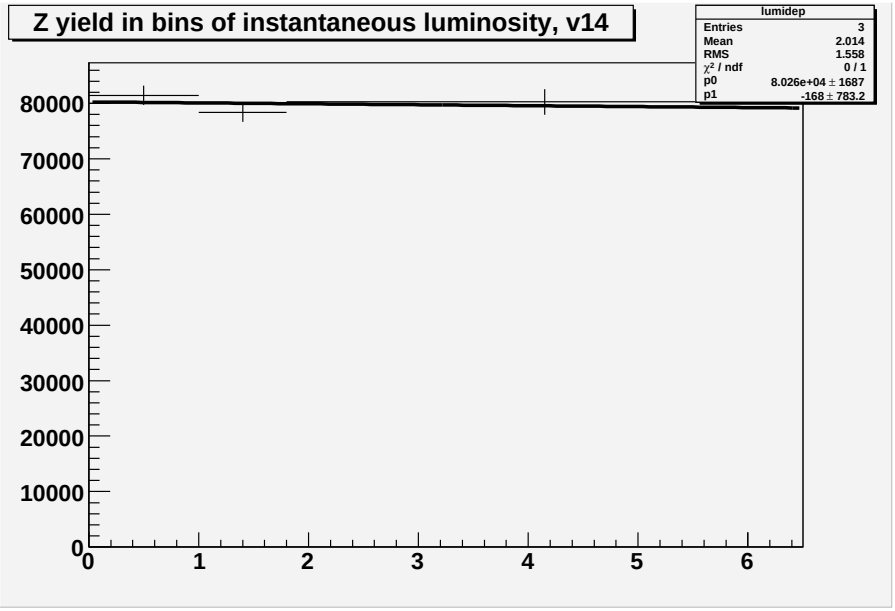

Figure 19: Sum of Z yields in three instantaneous luminosity bins derived from data epochs v14a–c, divided by a normalized integrated luminosity fraction. The error bars indicate the statistical uncertainties of selection and efficiency determination. The distribution is compatible with being flat, as indicated by the slope of the superimposed linear fit. A constant value fit results in a χ^2/dof of 1.6/2.

	trigger	yield Y	total % error
v08	2MU_A_L2M0	$1144.0^{+85.7}_{-83.5}$	$^{+7.49}_{-7.30}$
v09	2MU_A_L2M0	$6088.0^{+370.8}_{-256.3}$	$^{+6.09}_{-4.21}$
v10	2MU_A_L2M0	$2721.0^{+260.4}_{-135.2}$	$^{+9.57}_{-4.97}$
v11	MUW_W_L2M3_TRK10	$15658.0^{+507.1}_{-443.0}$	$^{+3.24}_{-2.83}$
v12a	MUW_W_L2M3_TRK10	$11342.0^{+604.1}_{-748.2}$	$^{+5.33}_{-6.60}$
v12b	MUW_W_L2M3_TRK10	$22099.0^{+641.5}_{-1129.1}$	$^{+2.90}_{-5.11}$
v12c	MUW_W_L2M3_TRK10	$22361.0^{+679.8}_{-788.8}$	$^{+3.04}_{-3.53}$
v13a	DMU1_LM6	$13337.0^{+466.8}_{-743.0}$	$^{+3.50}_{-5.57}$
v13c	MUH1_TK12_TLM12	$27803.0^{+1760.0}_{-706.7}$	$^{+6.33}_{-2.54}$
v13d	MUH1_TK12_TLM12	$17491.0^{+1147.5}_{-515.4}$	$^{+6.56}_{-2.95}$
v13e	MUH1_TK12_TLM12	$24603.0^{+726.2}_{-651.9}$	$^{+2.95}_{-2.65}$
v14a	MUH1_TK12_TLM12	$39977.0^{+1112.1}_{-957.9}$	$^{+2.78}_{-2.40}$
v14b	MUH1_TK12_TLM12	$15908.0^{+567.0}_{-576.8}$	$^{+3.56}_{-3.63}$
v14c	MUH1_TK12_TLM12	$21081.0^{+644.8}_{-1042.4}$	$^{+3.06}_{-4.94}$

Table 7: Yields for the different trigger epochs. The trigger used for the central value of the yield is also indicated.

9 Results

Table 7 gives the fully corrected yield for all data periods, along with estimated uncertainties. Tables 8 – 11 detail statistical and systematic error contributions to the yield for all epochs.

	v08	**v09**	**v10**	**v11**	**v12a**	**v12b**	**v12c**
σ_{data} (%)	± 7.04	± 3.05	± 4.57	± 1.68	± 2.03	± 1.39	± 1.38
σ_{MCstat} (%)	± 0.18	± 0.18	± 0.18	± 0.18	± 0.18	± 0.18	± 0.18
$\sigma_{\mu\text{ID}}$ (%)	± 0.91	± 0.91	± 0.92	± 1.09	± 1.35	± 0.87	± 0.91
$\sigma_{\mu\text{TRK}}$ (%)	± 0.62	± 0.61	± 0.61	± 0.77	± 0.94	± 0.71	± 0.71
$\sigma_{\mu\text{SMR}}$ (%)	$^{+0.69}_{-0.27}$	$^{+0.68}_{-0.29}$	$^{+0.68}_{-0.31}$	$^{+0.65}_{-0.23}$	$^{+0.65}_{-0.22}$	$^{+0.58}_{-0.26}$	$^{+0.54}_{-0.29}$
$\sigma_{\mu p_T\text{SMR}}$ (%)	$^{+0.43}_{-0.01}$	$^{+0.42}_{-0.03}$	$^{+0.42}_{-0.00}$	$^{+0.45}_{-0.03}$	$^{+0.38}_{-0.01}$	$^{+0.36}_{-0.08}$	$^{+0.30}_{-0.11}$
σ_{BEAM} (%)	$^{+1.04}_{-0.27}$	$^{+1.06}_{-0.58}$	$^{+1.05}_{-0.24}$	$^{+1.07}_{-0.25}$	$^{+1.06}_{-0.24}$	$^{+1.38}_{-0.23}$	$^{+0.85}_{-0.78}$
σ_{acc}	$^{+1.39}_{-0.00}$	$^{+4.80}_{-0.00}$	$^{+7.88}_{-0.00}$	$^{+1.39}_{-0.00}$	$^{+4.13}_{-0.19}$	$^{+1.01}_{-0.81}$	$^{+1.70}_{-0.00}$
$\sigma_{\text{NLO+PDF}}$ (%)	$^{+0.72}_{-1.07}$	$^{+0.73}_{-1.08}$	$^{+0.74}_{-1.08}$	$^{+1.07}_{-1.48}$	$^{+1.09}_{-1.47}$	$^{+1.10}_{-1.49}$	$^{+1.13}_{-1.50}$

Table 8: Summary of yield uncertainties from all sources except triggers for epochs v08-v12c. σ_{data} is the statistical error from the number of candidates in the data. σ_{MCstat} is the binomial Monte Carlo statistics error. $\sigma_{\mu\text{acc}}$ is a systematic error from varying acceptance. $\sigma_{\mu\text{ID}}$ is statistical error on muon identification efficiency from the tag and probe method. $\sigma_{\mu\text{TRK}}$ is the statistical error on muon tracking from the tag and probe method. $\sigma_{\mu\text{SMR}}$ is systematic error due to varying the multiple Coulomb scattering term in the muon resolution function. $\sigma_{\mu p_T\text{SMR}}$ is systematic error due to varying the spectrometer term in the muon resolution function. σ_{BEAM} is the systematic error estimated from varying the beam shape profile. σ_{LUMI} is the systematic error estimated from varying the luminosity profiles. $\sigma_{\text{NLO+PDF}}$ is the systematic error estimated from varying the NLO PDF.

	v13a	**v13c**	**v13d**	**v13e**	**v14a**	**v14b**	**v14c**
σ_{data} (%)	± 1.97	± 1.36	± 1.65	± 1.40	± 1.06	± 1.77	± 1.48
σ_{MCstat} (%)	± 0.18	± 0.15	± 0.15	± 0.15	± 0.15	± 0.15	± 0.15
$\sigma_{\mu\text{ID}}$ (%)	± 1.03	± 0.76	± 0.93	± 0.85	± 0.77	± 1.46	± 1.31
$\sigma_{\mu\text{TRK}}$ (%)	± 0.84	± 0.65	± 0.89	± 0.72	± 0.68	± 1.18	± 1.11
$\sigma_{\mu\text{SMR}}$ (%)	$^{+0.54}_{-0.40}$	$^{+0.57}_{-0.39}$	$^{+0.09}_{-0.39}$	$^{+0.55}_{-0.42}$	$^{+0.56}_{-0.40}$	$^{+0.55}_{-0.39}$	$^{+0.57}_{-0.39}$
$\sigma_{\mu p_T\text{SMR}}$ (%)	$^{+0.18}_{-0.10}$	$^{+0.00}_{-0.04}$	$^{+0.00}_{-0.02}$	$^{+0.00}_{-0.03}$	$^{+0.00}_{-0.02}$	$^{+0.00}_{-0.00}$	$^{+0.00}_{-0.04}$
σ_{BEAM} (%)	$^{+0.82}_{-0.75}$	$^{+0.68}_{-0.86}$	$^{+0.61}_{-1.00}$	$^{+0.77}_{-0.88}$	$^{+0.77}_{-0.89}$	$^{+0.95}_{-0.87}$	$^{+0.67}_{-1.14}$
σ_{acc}	$^{+1.75}_{-0.03}$	$^{+2.37}_{-0.02}$	$^{+2.03}_{-0.42}$	$^{+0.66}_{-0.25}$	$^{+1.30}_{-0.00}$	$^{+0.73}_{-0.50}$	$^{+0.33}_{-0.92}$
$\sigma_{\text{NLO+PDF}}$ (%)	$^{+0.91}_{-1.12}$	$^{+1.17}_{-1.33}$	$^{+1.15}_{-1.32}$	$^{+1.17}_{-1.36}$	$^{+1.15}_{-1.35}$	$^{+1.18}_{-1.39}$	$^{+1.16}_{-1.34}$

Table 9: Summary of yield uncertainties from all sources except triggers for epochs v13a-v14d. σ_{data} is the statistical error from the number of candidates in the data. σ_{MCstat} is the binomial Monte Carlo statistics error. $\sigma_{\mu\text{acc}}$ is a systematic error from varying acceptance. $\sigma_{\mu\text{ID}}$ is statistical error on muon identification efficiency from the tag and probe method. $\sigma_{\mu\text{TRK}}$ is the statistical error on muon tracking from the tag and probe method. $\sigma_{\mu\text{SMR}}$ is systematic error due to varying the multiple Coulomb scattering term in the muon resolution function. $\sigma_{\mu p_T\text{SMR}}$ is systematic error dueto varying the spectrometer term in the muon resolution function. σ_{BEAM} is the systematic error estimated from varying the beam shape profile. σ_{LUMI} is the systematic error estimated from varying the luminosity profiles. $\sigma_{\text{NLO+PDF}}$ is the systematic error estimated from varying the NLO PDF.

trigger	v08	v09	v10	v11	v12a	v12b	v12c
l1atxx_loose	±1.08	±1.08	±1.08				
l2m0_loose_l1atxx	±0.08	±0.08	±0.08				
l1wtlx_loose				±0.74	±0.95	±0.64	±0.65
l2m3_loose_l1wtlx				±0.43	±0.58	±0.32	±0.37
l3trk10_trackloose				±0.48	±0.57	±0.35	±0.38
Trigger Variation	$^{+0.00}_{-2.02}$	$^{+0.00}_{-2.02}$	$^{+1.95}_{-0.00}$	$^{+0.23}_{-0.29}$	$^{+0.00}_{-3.95}$	$^{+0.00}_{-3.95}$	$^{+0.00}_{-3.95}$

Table 10: Trigger-related uncertainties (%) for trigger epochs v08-v12c. The top 5 rows list the statistical errors on independent trigger terms for each global trigger, as determined by tag and probe methods. The last row shows the variation in the yield obtained from comparing the results from separate global triggers for the same epoch. A blank table entry indicates that the particular contribution is not present for the epoch.

trigger	v13a	v13c	v13d	v13e	v14a	v14b	v14c
l1atxx_loose	±1.25						
l2m0_loose_l1atxx	±0.20						
l3l6_loose_l1atxx_l2m0	±0.24						
l1trk10_trackloose		±0.55	±0.61	±0.52	±0.45	±0.93	±0.63
l1wtxx_loose		±0.48	±0.56	±0.50	±0.46	±0.89	±0.78
l3cml12_loose_l1wtxx_l3l0_l3trkxh10					±0.27	±0.64	±0.56
l3l0_loose_l1wtxx		±0.27	±0.33	±0.29	±0.25	±0.61	±0.51
l3trk12h10_trackloose_l1trk10		±0.55	±0.61	±0.54	±0.45	±0.67	±0.65
L3 matching		±0.15	±0.18	±0.16			
Trigger Variation	$^{+0.00}_{-4.66}$	$^{+3.76}_{-0.00}$	$^{+3.76}_{-0.00}$	$^{+3.76}_{-0.00}$	$^{+0.00}_{-0.71}$	$^{+0.00}_{-0.71}$	$^{+0.00}_{-0.71}$

Table 11: Trigger-related uncertainties (%) for trigger epochs v13a-v14c. The top 8 rows list the statistical errors on independent trigger terms for each global trigger, as determined by tag and probe methods. The next-to-last row shows the estimated uncertainty associated with matching level 3 tracks to offline tracks, applicable only for epochs v13c-v13e. The last row shows the variation in the yield obtained from comparing the results from separate global triggers for the same epoch. A blank table entry indicates that the particular contribution is not present for the epoch.

References

[1] E. Nurse and P. Telford, DØ Note 4573, "Measurement of the Cross section for Inclusive Z Production in Dimuon Final States at $\sqrt{s} = 1.96$ TeV" (analysis note), Aug. 11, 2004; and DØ Note 4573, Jan. 20, 2005 (conference note).

[2] G. Borissov, H. Greenlee, M. Hildreth, K. Hanagaki, A. Kharchilava, S. Kulik, M. Zdrazil, DØ Note 4161, 'The P14 Tracker Realignment'.

[3] http://www-d0.fnal.gov/computing/algorithms/muon/p17/certification_link.htm. The analysis note is still in preparation.

[4] G. Hesketh *et al.*, "Content of the p17 Muon Thumbnail", DØ Note 4735, Feb. 26, 2005.

[5] G. Hesketh, "Muon Isolation and QCD Backgrounds for W and Z", DØ Note 5177, July 13, 2006.

[6] Private communication, Marco Verzocchi.

[7] http://www-d0.fnal.gov/Run2Physics/wz/d0-private/wzskim/

[8] D. Whiteson and M. Kado, DØ Note 4070, 'Muon Isolation Studies'.

[9] S. Eno and M. Verzocchi, DØ Note 4097, 'Status of the Fast Simulation, PMCS'

[10] T. Sjöstrand *et al.*, Computer Physics Commun 135 (2001) p238, 'Pythia v6.2 Physics and Manual'.

[11] H. Schellman, "The Longitudinal Shape of the Luminous Region at DØ", June 12, 2006.

[12] J. Pumplin et al, hep-ph/0201195 'New Generation of Parton Distributions with Uncertainties from Global QCD Analysis'

[13] E. Nurse and P. Telford, DØ Note 4114, 'Measurement of $\sigma \cdot Br$ for $Z \longrightarrow \mu^+\mu^-$ in $p\bar{p}$ collisions at 1.96 TeV.'

[14] C.R. Hamberg, W.L. van Neerven and T. Matsuura, Nucl. Phys. B359 (1991) 343.

[15] add RESBOS reference here

[16] add reference for RESBOS data/MC agreement here (Lei Wang's D0note? Terry Toole?)

[17] H. Schellman, DØ Note 5243, version 5.0

Acknowledgements

This note has been built around the framework produced by Emily Nurse and Paul Telford. The authors wish to thank Tim Bolton, Volker Büscher, Harald Fox, Georgy Golovanov, Jon Hays, John Hobbs, Rick van Kooten, Dmitri Onoprienko, Slava Sharyy, Raimund Ströhmer, Boris Tuchming, Sahal Yacoob, Taka Yasuda and Terry Wyatt for helpful discussions and their contributions to text and software needed for this analysis.

A Software versions

The figures and numbers presented in this note were created with the following set of software packages:

CAFtree production

- D0RunII base release p18.07.00
- cps_evt
- d0root_nnbtag
- em_evt
- em_util
- jetreco
- lm_access
- tau_tmb
- thumbnail
- tmb_analyze (rcp modification: do not run b-tagging)
- tmb_tree_maker

efficiency determination

- D0RunII base release p18.07.00
- dq_defs v2006-05-04
- dq_util v02-00-00
- edm_dq v02-00-00
- eff_utils v01-10-02
- muid_eff v02-00-00 (modification: coarser binning for efficiency histograms)
- muo_cert v04-00-22 (modifications: Z mass cut, muon $p_t > 20\,\mathrm{GeV}/c$, cut on z coordinate of MC Z production vertex, use data quality selection with blinding)
- wzreco v04-00-22 (modification: require Z mass $> 70\,\mathrm{GeV}/c^2$)
- wzcross_dq v00-01-11
- wzcross_sample v00-01-00

MC efficiency reweighting

- D0RunII base release p18.08.00
- eff_utils v01-11-05
- muid_eff v02-00-00
- wzmuxsec v01-12-03

event selection

- D0RunII base release p18.08.00
- caf_dq v02-01-01
- caf_eff_utils v01-09-03
- caf_pdfreweight v00-00-04
- caf_trigger v04-00-02
- caf_util v03-02-02 (MuonSelector modification: z cut)
- cafe p18-br-88
- cafe_sam p18-br-03
- dq_defs v2006-05-04
- dq_util v02-01-01
- eff_utils v01-11-05
- emid_cuts v02-04-08
- jetcorr v07-02-12
- kinem_util p17-br-01
- met_util p17-br-01
- muid_eff v02-00-00
- tmb_tree p18-br-75
- wz_cafreco v00-05-05
- wzcross_dq v00-01-11
- wzcross_sample v00-01-08 (modification: use only BeamWeight class)
- wzmuxsec v01-12-03